Trabajo Fin de Máster
Máster en Diseño Avanzado en Ingeniería Mecánica

Numerical Computation of the Unsteady Linearized Potential Flow past Airfoils in Compressible Subsonic Regime by Finite Differences Methods

Autor: Manuel Colera Rico

Tutor: Miguel Pérez-Saborid Sánchez-Pastor

Dep. Ingeniería Aeroespacial y Mecánica de Fluidos
Escuela Técnica Superior de Ingeniería
Universidad de Sevilla

Sevilla, 2016

Trabajo Fin de Máster
Máster en Diseño Avanzado en Ingeniería Mecánica

Numerical Computation of the Unsteady Linearized Potential Flow past Airfoils in Compressible Subsonic Regime by Finite Differences Methods

Autor:

Manuel Colera Rico

Tutor:

Miguel Pérez-Saborid Sánchez-Pastor

Profesor Titular

Dep.Ingeniería Aeroespacial y Mecánica de Fluidos

Escuela Técnica Superior de Ingeniería

Universidad de Sevilla

Sevilla, 2016

A mi familia, en especial, a mis padres, y a mis amigos

Acknowledgements

I would like to express my gratitude to professor Miguel Pérez-Saborid for initiating me in the world of computational fluid dynamics during the last years, and for his great dedication and advice along this work.

I also thank my parents for their support and their magnificent guidance —both in technical and human aspects— during all these years, as well as my aunt Inma for her brilliant pieces of advice about writing technical essays.

Finally, I am grateful to all my friends for making the University one of my very best experiences.

The author

Contents

Introduction

Motivation, aims and applications

The interest for unsteady aerodynamic flows has increased in the recent years due to its many applications. For example, in aeronautics it is of primordial importance to know the extra loads over an aeroplane that suddenly changes its angle of attack, enters in a gust or goes into a turbulence zone. In addition, many aeroelastic problems can appear such as the divergence and the flutter of wings or other aerodynamic surfaces. In biomedicine, snoring problems are studied by analysing the unsteady oscillations of the vocal chords produced by the air that passes through the throat. Aeroelastic problems are also of interest in civil engineering, where wind can cause flutter in tall bridges and buildings as happened, for example, in the famous case of the failure of the Tacoma Bridge (figure 1).

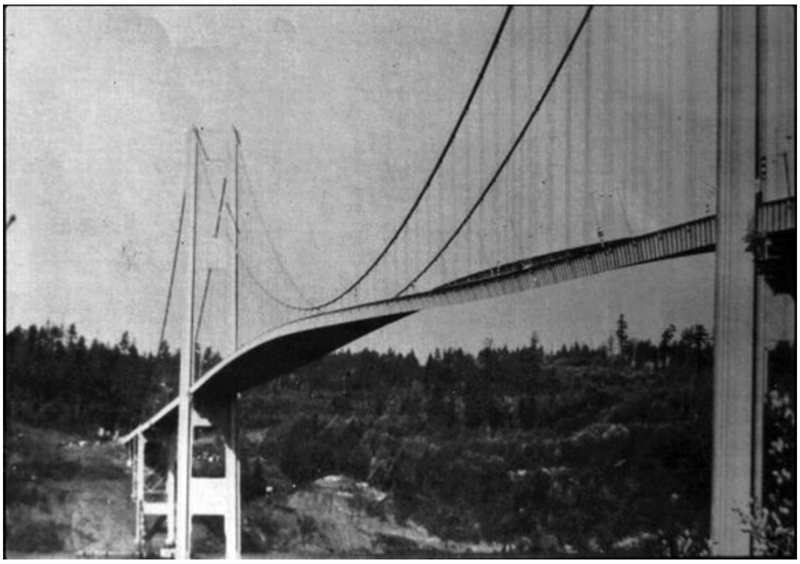

Figure 1: Flutter problem at the Tacoma Bridge, that caused its destruction later. Photography obtained from https://en.wikipedia.org/wiki/Tacoma_Narrows_Bridge_(1940).

Usually, many of those phenomena (such as snoring and wing flutter) are not modelled directly as three-dimensional problems. Instead, according to the strip theory [9], the corresponding entity (the vocal cords or the wing) is divided into cross sections that are studied as if they were subject to a two-dimensional flow. Using this approximation, the linearized potential theory for flows past airfoils was developed around 1940. This theory yields simple equations whose physical meaning is very clear. However, this transparency was soon lost since, due to the absence of efficient computers in those times, the equations had to be solved analytically —usually in the frequency domain—, leading to tedious mathematical developments whose physical meaning is difficult to grasp and disorientate the interested students, especially when air compressibility is taken into account. Furthermore, many of those developments —which are still used as a reference in the specialized literature— are only valid for particular cases such as harmonic motion, sudden changes in the angle of attack, sharp edge gusts, etc.

Since computers have experienced a great development in the last years, some efforts have been made to solve numerically the linearized, unsteady potential equations in an easier and more direct way, which is valid for any motion of the airfoil and uses the more physically intuitive time domain approach. For example, Katz and Plotkin [15] developed a marching-time vortex-lattice method for incompressible flow that was able to calculate the forces over an airfoil when its motion was known, and Hernandes and Soviero [12][13] presented a similar method suitable for compressible flow. Both methods were studied and improved by Colera and Pérez-Saborid [6], who proposed two truncation algorithms in order to reduce their computational cost. These authors also coupled the equations of the vortex-lattice methods with those of the airfoil dynamics for studying problems were the airfoil motion is the unknown as happens, for example, in the problem of flutter.

Although the Hernandes-Soviero method is precise and valid for general two-dimensional problems, it presents some drawbacks:

- A good comprehension of not well-known aspects such as the induced velocity field of unsteady compressible vortexes, the piston theory and the auto-induced velocities of an unsteady vortex in supersonic flow is required.
- The method is constructed by means of the unsteady compressible vortex, a fundamental solution that presents a lack of physical meaning, as pointed in [6].
- It is a marching-time method which has to keep track of the solutions corresponding to many previous times in order to compute the solution at some given instant. Thus, it can run very slowly even with the truncation method developed in [6].
- Its extension to the three-dimensional regime is not clear, despite some works have been done on the matter [19].

The disadvantages that vortex-lattice methods pose in the case of compressible unsteady flows past airfoils have motivated the consideration in this work of an alternative marching-time method that is not based on the use of unsteady compressible vortexes or any other fundamental solutions, but on discretizing the differential equations of the linearized potential flow theory directly by finite differences. Originally, this method was proposed by Hariharan, Ping and Scott [11], who used an uniform grid to mesh the fluid domain and an explicit time integration scheme. Despite providing good accuracy and being easy to understand and implement, this method, as presented by these authors, makes necessary to use a very thin mesh to get good results, as well as a very small time step in order to avoid instabilities. Also, the method was implemented for the case when the motion of the airfoil is given, but not when it is just the unknown as in flutter problems.

All of this has motivated the present work, whose main **objectives** are:

- To propose a modification for the Hariharan-Ping-Scott method that uses a non-uniform mesh and an implicit time integration scheme, leading to better accuracy and stability. This modification will be just named as *modified Hariharan-Ping-Scott method* in this work, and its efficiency will be compared with the Hernandes-Soviero vortex-lattice modified with the truncation algorithm proposed by Colera and Pérez-Saborid [6]. Similarly, the latter method will be named as *modified Hernandes-Soviero method* in this work.

- To couple the modified Hariharan-Ping-Scott method with the airfoil dynamics in order to compute its motion when it is unknown. This coupling algorithm will be named *coupled Hariharan-Ping-Scott method* along this work.

As applications of the above mentioned methods, some results of interest that are very difficult to obtain analytically have been computed like, for example, the extra lift that appears after a sudden change of the angle of attack or after a sharp-edge gust, which could be of interest for structural calculations. Also, the wake evolution, that can seriously affect the behaviour of aeroplanes or turbomachine blades, has been computed for the two-dimensional case. The flutter point of rigid and flexible airfoils has also been considered and, apparently, this is first self-consistent numerical analysis of the compressible, linearized coupled dynamics of the fluid-airfoil system carried out in the literature. Furthermore, for the flutter of a flexible airfoil in compressible flow, no references have been found in the available literature to make comparisons with, thus, the results presented here for that case are original or not well-known.

(a) (b)

Figure 2: Asymmetric flutter mode in a glider (a) and wake after an aeroplane that can seriously affect the control of incoming ones (b).

The methods analysed in this work can be easily and efficiently implemented with programs like Matlab, which has simple syntax rules, is well-known by students and has many mathematical libraries that allow a friendlier implementation. Also, they make use of the physics beyond the basic equations of the unsteady linearized potential theory, never leaving the time domain. Thus, they are very intuitive (unlike the classical frequency domain approach) and can be very useful for teaching applications. Also, since they are efficient, precise and permit the calculation of many variables of interest, they can be used for the preliminary design of wings and helicopter blades or for any other situation where the computation based on CFD commercial programs is too expensive for the required precision.

Finally, this work is a way to put into practice some concepts learned in the Master Degree in Advanced Design in Mechanical Engineering, such as linear waves in gas dynamics, classic mechanics and computational methods (sparse matrixes, LU factorization and BDF for ordinary differential equations).

Structure and main contributions

This work is mainly structured in three chapters. In the first one, some general concepts are to be introduced such as the principal equations of the linearized potential theory of flows past airfoils, some finite differences formulas for non-uniform meshes and a non-reflecting boundary condition for the convected wave equation.

In the second chapter, those general concepts are to be used in order to explain the modified Hariharan-Ping-Scott method. As commented before, this method differs from the original one in that it uses a non-uniform grid and an implicit time integration scheme, being then more accurate and stable. These improvements are original and therefore they constitute one of the main contributions of this work. Some problems of interest will be solved with the method and its efficiency and convergence will be compared with the Hernandes-Soviero method's.

In the third chapter, the modified method is to be coupled with the airfoil dynamics in order to compute its motion in the case in which it is the unknown. Again, this coupling method is original and therefore it is another contribution of this work. With the coupled method, some problems related to the flutter of rigid and flexible airfoils and to the response to a gust are to be solved. As pointed before, no results have been found in the available literature to compare with the obtained ones in the case of the flutter of a flexible airfoil. Hence, those results are original or not well-known and are one of the main contributions of this work as well.

Finally, the bibliography consulted for this work is included.

Chapter 1

General equations and considerations

1.1. Introduction

In this chapter some general ideas are to be introduced briefly before approaching the explanation of the numerical methods in the following chapters. First, some simplifications involving the fluid and the airfoil and also the equations that govern the flow are shown in section 1.2. Second, the calculation of the lift, the pitching moment and other generalized forces over the airfoil by means of the fluid variables is explained in section 1.3. Later, some finite differences formulas for non-uniform meshes that will be implemented in the numerical methods are derived in section 1.4. Finally, an additional boundary condition for finite domains is obtained in section 1.5 following the same reasoning that Hariharan, Ping and Scott [11].

1.2. Linearized potential flow equations

Consider an airfoil —which is two-dimensional by definition— in the sine of an horizontal, constant and uniform flow of speed U_∞ that presents vertical motion and/or is submitted to a gust whose vertical speed is w_g (as shown in figure 1.1), and assume the following hypothesises, valid for the most part of practical cases:

- The Reynolds number based on the chord lenght c of the airfoil and the properties of the fluid upstream is very high, so viscous effects can be neglected except in the boundary layer of the airfoil and in the wake.
- Gravity forces and heat transfer are neglected as well.
- The amplitude of the airfoil motion and the gust intensity are small, i.e., their speeds are much lower than U_∞ and the displacements of the airfoil are much lower than c.
- The airfoil's thickness is much lower than its chord c.
- The boundary layer of the airfoil remains adhered to it.

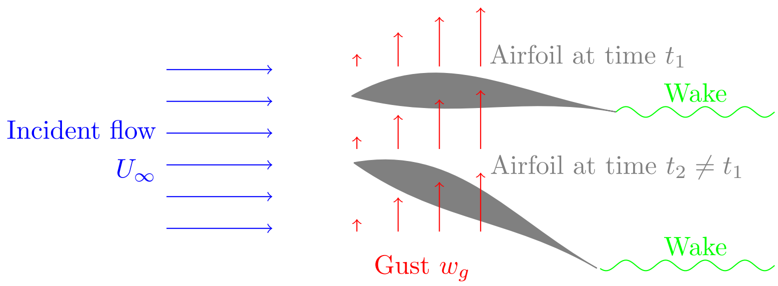

Figure 1.1: Scheme of an airfoil in the sine of an uniform incident flow U_∞ that presents vertical motion and/or is submitted to a gust whose vertical speed is w_g.

With these assumptions, the linearized potential theory can be used to describe the flow around the airfoil. This theory, that is explained in references [3],[6],[10], can be summarized in a few concepts. First of all, the airfoil and the wake are placed in the x axis (which is parallel to the incident flow), the first between the coordinates $x = 0$ and $x = c$ and the latter between $x = c$ and $x \to \infty$ (see figure 1.2). The y axis is defined perpendicular to the x axis, and the thicknesses of the airfoil and the wake are ignored. The remaining space is occupied by a non-viscous and irrotational fluid.

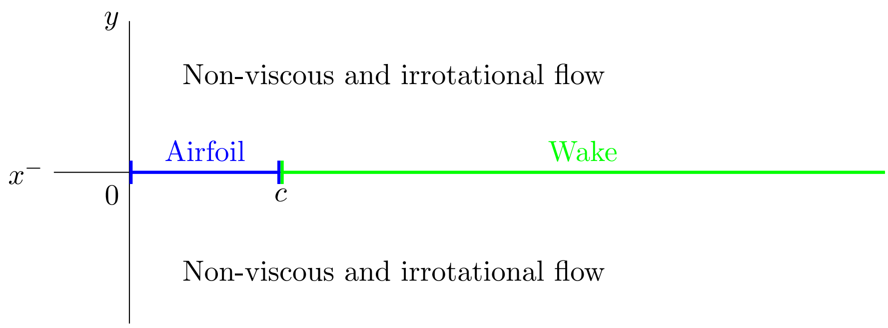

Figure 1.2: Diagram of the flow field simplification made by the linearized potential theory.

Second, all the properties of the fluid like the velocity $\mathbf{v}$, pressure p, density ρ, etc. are written as their values upstream ($U_\infty \mathbf{u_x}$, p_∞, ρ_∞) plus a small perturbation, i.e.:

$$\mathbf{v} = U_\infty \mathbf{e_x} + \mathbf{v}'; \quad p = p_\infty + p'; \quad \rho = \rho_\infty + \rho'$$

where:

$$|\mathbf{v}|' \ll U_\infty; \quad p' \ll p_\infty; \quad \rho' \ll \rho_\infty$$

Third, considering that the flow is irrotational ($\nabla \times \mathbf{v} = 0$), it is shown that all the perturbation variables can be extracted from just one variable, that is the fluid perturbation potential[1] ϕ. In particular, the perturbation speed and the perturbation pressure are related to that potential by the following relationships:

$$\mathbf{v}' = \nabla \phi \tag{1.1}$$

$$p' = -\rho_\infty \left(\frac{\partial \phi}{\partial t} + U_\infty \frac{\partial \phi}{\partial x} \right) \tag{1.2}$$

[1] Usually, it will be just called *potential* and not *perturbation potential*.

In unsteady problems, the potential is antisymmetric respect to the x axis (inducing an antisymmetric perturbation velocity $\mathbf{v}'$ as well), being continuous at $x < 0$, $y = 0$ and presenting a jump across the line occupied by the airfoil and the wake ($x > 0$, $y = 0$). Thus, it is only necessary to calculate the potential in the upper half plane ($y > 0$).

It has to be noticed that, due to that antisymmetry, $\phi(x, 0^+) = \phi(x, 0^-) = 0$ at least when $x < 0$. However, it is important to remark that the latter relation can be extended to the point $x = 0$, because ϕ is continuous in that point. Indeed, there is a well-known leading edge suction, that takes place at $x = y = 0$, and is characterized by a vortex density γ that behaves as $1/\sqrt{x}$. It can be shown [6] that this vortex density is proportional to the horizontal perturbation velocity $u = \partial\phi/\partial x$ so, in the vecinities of the point $x = y = 0$, ϕ has to behave as $\sqrt{x}$, as shown in figure 1.3. Therefore, ϕ is continuous at $x = y = 0$ (although it presents an infinite slope there) and it is possible to say that:

$$\phi(x, 0^+) = \phi(x, 0^-) = 0; \quad x \le 0 \tag{1.3}$$

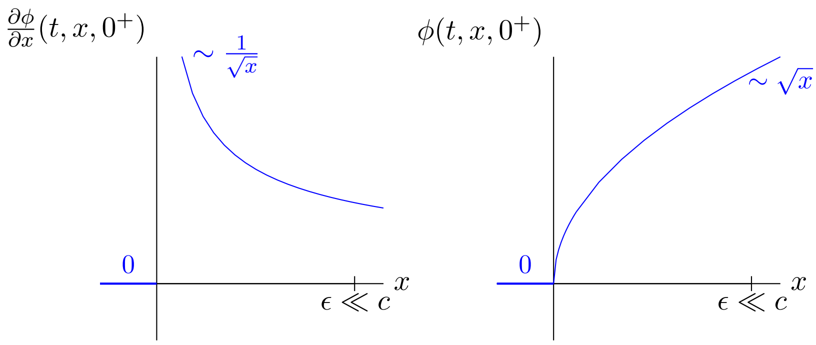

Figure 1.3: Illustration of the asymptotic behaviour of $\partial\phi/\partial x$ and ϕ nearby $x = y = 0$ due to the presence of the well-known leading edge suction. As can be seen, the mentioned suction does not imply any discontinuity for ϕ in that point.

The equation that governs the potential ϕ in the fluid domain is the convected wave equation:

$$\left(\frac{\partial}{\partial t} + U_\infty \frac{\partial}{\partial x}\right)^2 \phi = a_\infty^2 \nabla^2 \phi \tag{1.4}$$

where a_∞ is the upstream sound speed. In order to develop the numerical code presented in this work, it is convenient to rewrite the latter equation in the following way:

$$\frac{\partial^2\phi}{\partial t^2} = -2U_\infty \frac{\partial^2\phi}{\partial t\,\partial x} + \left(a_\infty^2 - U_\infty^2\right)\frac{\partial^2\phi}{\partial x^2} + a_\infty^2 \frac{\partial^2\phi}{\partial z^2} \tag{1.5}$$

The boundary conditions for the potential are:

- Non-penetration of the fluid in the airfoil's surface:

$$\frac{\partial\phi}{\partial z} = \frac{\partial z_p}{\partial t} + U_\infty \frac{\partial z_p}{\partial x} - w_g(t, x); \quad 0 \le x \le c; \quad y = 0^+ \tag{1.6}$$

  where $z_p = z_p(t, x)$ is the displacement of the mean geometrical line of the airfoil respect from its steady position.

- Non-perturbed conditions at infinity:

$$\nabla\phi = 0; \quad x, y \to \infty; \tag{1.7}$$

- Kutta's condition (applies to the wake):

$$\frac{\partial\phi}{\partial t} + U_\infty \frac{\partial\phi}{\partial x} = 0; \quad x > c; \quad y = 0^+ \tag{1.8}$$

The equations (1.5)-(1.8) are to be solved by the modified Hariharan-Ping-Scott method presented here to get the fluid field around the airfoil.

1.3. Lift, pitching moment and other generalized forces

Once the perturbation potential ϕ is found, it is of great interest to calculate the actuating lift and pitching moment[2] over the airfoil.

If the upper surface of the airfoil ($0 \le x \le c$, $y = 0^+$) is denoted by *up*, and the lower one ($0 \le x \le c$, $y = 0^-$) by *down*, the lift l can be expressed as:

$$l = \int_{x=0}^{x=c} \left(p^{down} - p^{up}\right) dx$$

Using now the relations (1.2)-(1.3) and the fact that ϕ is antisymmetric, the latter equation reads as follows:

$$l = 2\rho_\infty \int_0^c \frac{\partial\phi^{up}}{\partial t} dx + 2\rho_\infty U_\infty \phi^{up}(t, x = c) \tag{1.9}$$

which is the generalized Kutta-Joukowski formula.

On the other hand, the pitching moment m_{le} over the leading edge (defined as positive if it makes the airfoil move its leading edge down) can be obtained performing the following integral:

$$m_{le} = \int_{x=0}^{x=c} \left(p^{down} - p^{up}\right) x\, dx$$

Using again the equation (1.2) and the antisymmetry of ϕ, it is obtained that:

$$m_{le} = 2\rho_\infty \int_0^c \frac{\partial\phi^{up}}{\partial t} x\, dx + 2\rho_\infty U_\infty \int_0^c \frac{\partial\phi^{up}}{\partial x} x\, dx$$

For numerical reasons, it is convenient to integrate by parts the second term in the right side of the last equation. Regarding equation (1.3), it follows that:

$$m_{le} = 2\rho_\infty \int_0^c \frac{\partial\phi^{up}}{\partial t} x\, dx + 2\rho_\infty U_\infty c\, \phi^{up}(t, c) - 2\rho_\infty U_\infty \int_0^c \phi^{up} dx \tag{1.10}$$

Notice that using (1.10) instead of the equation before it is not necessary to derive the potential respect to x and therefore the obtained result is more accurate.

[2] Actually, it is not the lift and the pitching moment, but the lift and pitching moment per unit length. However, the term *per unit length* will be omitted in this work.

In some complex cases like, for example, flexible airfoils, their motion will be described in terms of some generalized coordinates $q_i(t)$ and their corresponding shape functions $\psi_i(x)$, i.e.:

$$z_p(t,x) = \sum_i \psi_i(x) q_i(t)$$

In those cases, it will be of interest to calculate the generalized aerodynamic forces Q_i associated with the different coordinates. The expression of the above mentioned Q_i can be obtained giving the airfoil a virtual displacement and calculating the virtual work of the aerodynamic pressure. In other words:

$$\delta W = \sum_i Q_i \delta q_i = \int_{x=0}^{x=c} \left(p^{down} - p^{up}\right) \delta z_p dx = \sum_i \int_{x=0}^{x=c} \left(p^{down} - p^{up}\right) \psi_i \delta q_i dx$$

Using the latter equation and the same procedure than the one used for calculating m_{le}, it follows that:

$$Q_i = 2\rho_\infty \int_0^c \frac{\partial \phi^{up}}{\partial t} \psi_i \, dx + 2\rho_\infty U_\infty \psi_i(c) \phi^{up}(t,c) - 2\rho_\infty U_\infty \int_0^c \phi^{up} \frac{d\psi_i}{dx} dx \tag{1.11}$$

The equations (1.9)-(1.11) will be used in the modified Hariharan-Ping-Scott method explained in the present work.

1.4. Finite differences for non-uniform meshes

In the method presented in this work, finite differences are to be used in a non-uniform mesh. Due to the fact that some of their expressions are not as intuitive and well-known as when the mesh is uniform, they are to be derived here first. In particular, the expressions of greatest interest for the present text and that are to be shown now are the backward, forward and central approximations to the first derivative, and the central approximation to the second derivative.

Backward approximation to the first derivative

Suppose a function $f(x)$ evaluated at three points named x_{i-2}, x_{i-1} and x_i (with $x_{i-2} < x_{i-1} < x_i$), and denote $f(x_j)$, $f'(x_j)$, $f''(x_j)$ and so on by f_j, f'_j, f''_j, etc.

According to the Taylor expansion, if f is smooth enough it can be said that:

$$f_{i-1} = f_i - f'_i \Delta x_1 + \frac{1}{2} f''_i \Delta x_1^2 - \frac{1}{6} f'''_i \Delta x_1^3 + O(\Delta x_1^4) \tag{1.12}$$

$$f_{i-2} = f_i - f'_i \Delta x_2 + \frac{1}{2} f''_i \Delta x_2^2 - \frac{1}{6} f'''_i \Delta x_2^3 + O(\Delta x_2^4) \tag{1.13}$$

where $\Delta x_1 = x_i - x_{i-1}$ and $\Delta x_2 = x_i - x_{i-2}$. Eliminating f''_i from the above equations, it is obtained that:

$$f'_i = f_i \frac{\Delta x_1 + \Delta x_2}{\Delta x_1 \Delta x_2} - f_{i-1} \frac{\Delta x_2}{\Delta x_1 (\Delta x_2 - \Delta x_1)} + f_{i-2} \frac{\Delta x_1}{\Delta x_2 (\Delta x_2 - \Delta x_1)} + O(\Delta x_2^2) \tag{1.14}$$

It can be checked that the error term in the latter equation involves the third derivative f'''_i and the error terms in equations (1.12)-(1.13); thus, it disappears if $f(x)$ is a second degree polynomial. In other words, the degree of precision of the formula (1.14) is 2.

Forward approximation to the first derivative

The forward approximation gives the value of f_i' by means of the value of f in three points called x_i, x_{i+1} and x_{i+2} (with $x_i < x_{i+1} < x_{i+2}$). It can be calculated from equation (1.14) replacing x_{i-1} by x_{i+1} and x_{i-2} by x_{i+2}, following that:

$$f_i' = -f_i \frac{\Delta x_1 + \Delta x_2}{\Delta x_1 \Delta x_2} + f_{i+1} \frac{\Delta x_2}{\Delta x_1 (\Delta x_2 - \Delta x_1)} - f_{i+2} \frac{\Delta x_1}{\Delta x_2 (\Delta x_2 - \Delta x_1)} + O(\Delta x_2^2) \quad (1.15)$$

where, now, Δx_1 and Δx_2 represent $x_{i+1} - x_i$ and $x_{i+2} - x_i$, respectively. Again, this formula has an accuracy degree equal to 2.

Centered approximation to the first derivative

In this case, f is evaluated at x_{i-1}, x_i and x_{i+1} (with $x_{i-1} < x_i < x_{i+1}$), and the aim is to compute f_i'. Proceeding again with the Taylor series, it can be written that:

$$f_{i-1} = f_i - f_i' \Delta x_- + \frac{1}{2} f_i'' \Delta x_-^2 - \frac{1}{6} f_i''' \Delta x_-^3 + O(\Delta x_-^4) \quad (1.16)$$

$$f_{i+1} = f_i + f_i' \Delta x_+ + \frac{1}{2} f_i'' \Delta x_+^2 + \frac{1}{6} f_i''' \Delta x_+^3 + O(\Delta x_+^4) \quad (1.17)$$

where $\Delta x_+ = x_{i+1} - x_i$ and $\Delta x_- = x_i - x_{i-1}$. Eliminating f_i'', it follows:

$$f_i' \simeq f_{i+1} \frac{\Delta x_-}{\Delta x_+ (\Delta x_+ + \Delta x_-)} + f_i \frac{\Delta x_+ - \Delta x_-}{\Delta x_+ \Delta x_-} - f_{i-1} \frac{\Delta x_+}{\Delta x_- (\Delta x_+ + \Delta x_-)} + O(\Delta x_+^2, \Delta x_-^2) \quad (1.18)$$

which is, as well, an approximation whose precision degree is 2.

Centered approximation to the second derivative

This approximation can be obtained if f_i' is eliminated from the system (1.16)-(1.17), leading to:

$$f_i'' = f_{i+1} \frac{2}{\Delta x_+ (\Delta x_+ + \Delta x_-)} - f_i \frac{2}{\Delta x_+ \Delta x_-} + f_{i-1} \frac{2}{\Delta x_- (\Delta x_+ + \Delta x_-)} + O(\Delta x_+, \Delta x_-) \quad (1.19)$$

which is, in the general case of non-uniform mesh ($\Delta x_- \neq \Delta x_+$), an approximation with precision degree equal to 2. It can be checked that, in the especial case of uniform mesh ($\Delta x_- = \Delta x_+$), the terms involving f_i''' in equations (1.16)-(1.17) cancel themselves when operating in order to obtain equation (1.19), and the error term in the latter becomes $O(\Delta x_+^2, \Delta x_-^2)$, as expected.

1.5. Non-reflecting boundary conditions

According to equation (1.4), the airfoil can be seen as a source of waves whose focus convects downstream with velocity U_∞ and whose front propagates with velocity a_∞ respect to that focus [6], as seen in figure 1.4. Since the real domain is infinite, these waves go away from the airfoil and never come back. However, it is imposible to simulate an infinite domain numerically, and, in practice, a big enough (but finite) domain has to be used instead. In that kind of domains, boundary condition (1.7) is not useful and has to be substituted by another one that makes waves not to reflect when arriving at the borders.

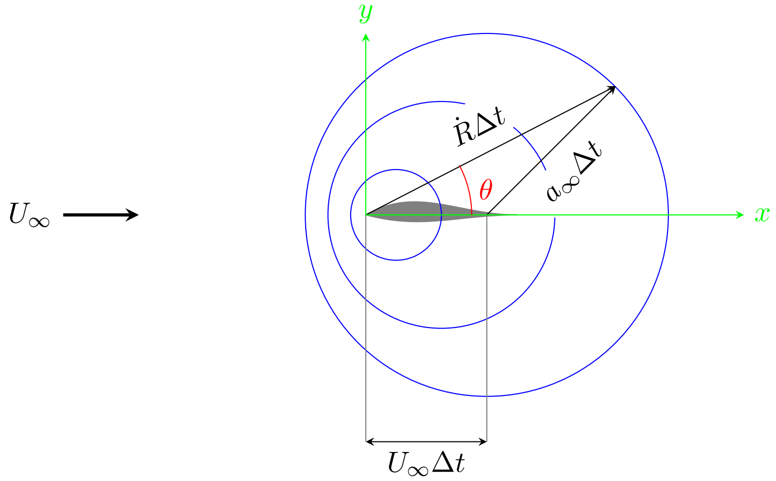

Figure 1.4: Wave propagation in subsonic flow. Δt is the lapse of time between the actual time t and the instant of birth of the wave.

Looking at the variables defined in figure 1.4, it follows that:

$$a_\infty^2 = \dot{R}^2 + U_\infty^2 - 2\dot{R}U_\infty \cos\theta$$

From this, and taking into account that $\dot{R}$ has to be positive when $\theta = 0, \pi$, it is obtained that:

$$\dot{R}(\theta) = U_\infty \cos\theta + \sqrt{a_\infty^2 - U_\infty^2 \sin^2\theta} \tag{1.20}$$

The wavefront, given in polar coordinates ($x = r\cos\theta$, $y = r\sin\theta$) by $r(\theta) = \dot{R}(\theta)\Delta t$, can be transformed into a cylindrical one by performing the following change of variables:

$$\hat{r} = \frac{a_\infty}{\dot{R}(\theta)} r; \quad \hat{\theta} = \theta$$

In the new system, the cylindrical wavefront propagates with velocity a_∞, and the far flow field can be approximated by the Friedlander asymptotic form [18]:

$$\phi \sim \frac{f(t - \hat{r}/a_\infty)}{\sqrt{r}}$$

which verifies:

$$\frac{\partial\phi}{\partial t} + a_\infty \left[\frac{\partial\phi}{\partial\hat{r}} + \frac{\phi}{2\hat{r}}\right] = 0$$

or, in terms of the original variables:

$$\frac{\partial\phi}{\partial t} + \dot{R}(\theta) \left[\frac{\partial\phi}{\partial x}\cos\theta + \frac{\partial\phi}{\partial y}\sin\theta + \frac{\phi}{2r}\right] = 0 \tag{1.21}$$

That is the differential form of the non-reflecting boundary condition that will be used in the finite domain considered in next chapters.

Chapter 2

Modified Hariharan-Ping-Scott method

2.1. Introduction

It was seen in the previous chapter that, under the assumptions of the linearized potential theory, the airfoil and the wake could be placed in the x^+ semiaxis and that all the fluid variables could be computed from another one called the potential (denoted by ϕ).

Now consider a rectangle in the upper half plane that surrounds the airfoil and part of the wake, and whose vertices are far enough from the airfoil (i.e., at a distance $\sim 10\,c$ from it). The main idea of the Hariharan-Ping-Scott method [11] is to mesh this rectangle into a grid of points and to discretize there the potential flow equations. If the potential is known at a certain instant t^n in the whole mesh, all the space derivatives can be computed by finite differences and therefore the time derivates can be calculated as well through the potential theory equations. Knowing the time derivatives, it is possible to obtain the potential in the mesh points at the following instant t^{n+1}, and so on until a final time t_f.

That Hariharan-Ping-Scott method uses an uniform mesh and an explicit time integration scheme. Although this formulation is easier to implement, it has as drawbacks that a very thin mesh is needed in order for the results to converge (sometimes leading to computer memory problems), and that a very small time step size has to be taken in order to avoid instabilities. Thus, two modifications are proposed here in order to improve those characteristics. They consist, respectively, in using a non-uniform mesh that concentrates more points where the potential presents a higher gradient —so such a thin mesh is no longer necessary— and in employing an implicit time integration scheme —that makes the method more stable and permits to take a much longer time step.

These modifications are to be explained first in section 2.2, where the main ideas are shown, the corresponding equations and matrixes are derived and some commentaries for its efficient implementation are made. Second, some results for typical problems in unsteady aerodynamics are computed and compared in section 2.3 with others obtained both theoretically and with the Hernandes-Soviero method [12][13] modified with the truncation algorithms proposed by Colera and Pérez-Saborid [6] (that were commented in the introductory chapter of this text). For simplicity reasons, the latter method will be named as *modified Hernandes-Soviero method*. After, a comparison of the convergence and the stability of the original and the modified Hariharan-Ping-Scott methods is done in section 2.4. Later, a brief study of the influence of the time step size in the convergence and the efficiency of both methods (modified Hariharan-Ping-Scott and modified Hernandes-Soviero) is done in section 2.5. Finally, some wake patterns for an harmonic movement of the airfoil have been computed in section 2.6.

To avoid possible confusions, it has to be pointed that, sometimes, the modified Hariharan-Ping-Scott and the modified Hernandes-Soviero methods will be called as finite differences method and vortex-lattice method, respectively, because that names emphasize the main ideas beyond them.

2.2. Description of the method

2.2.1. Main concepts

Consider a rectangular (but non-uniform) mesh like the one shown in the figure 2.1. Every point of the grid can be described by two indexes i, j, with $i = 1, \ldots, N_x$ and $j = 1, \ldots, N_y$, and also by a single index I that moves through the grid by rows, starting from the bottom one, and moving to the right inside each row. The relation between I and i, j is:

$$I = N_x(j-1) + i$$

There are two especial values of i: one for which the corresponding value of x is equal to 0 (say i_{le}) and another one for which the corresponding value of x is equal to c (say i_{te}). These two values represent the limits between which the airfoil is placed.

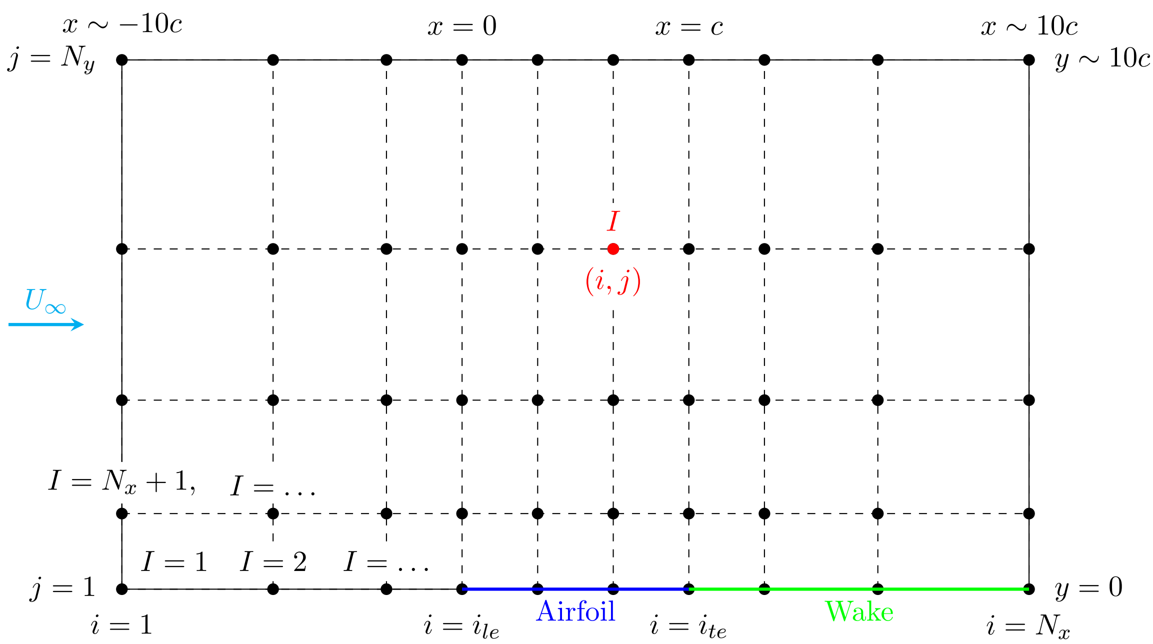

Figure 2.1: Scheme of the grid employed for the method.

The time is divided in uniform steps Δt, and every simulated instant is denoted by t^n. The potential evaluated at an instant t^n and at the point given by i, j is denoted by ϕ^n_{ij}. As every point can also be given by I, sometimes an abuse of notation will be done and the potential will be denoted by ϕ^n_I as well. The different values of ϕ^n_I can be grouped into a column vector $\boldsymbol{\phi}^n$ defined as:

$$\boldsymbol{\phi}^n = \left[\phi^n_1, \ldots, \phi^n_{N_\phi}\right]^T$$

where $N_\phi = N_x N_y$ is the total number of points in the grid.

Knowing $\boldsymbol{\phi}^n$ and $\boldsymbol{\phi}^{n-1}$, it is possible to define a value f^n_I (or f^n_{ij}) to every grid point that is:

- The second time derivative of ϕ at t^n ($\ddot{\phi}^n_I$) for the inner points ($i = 2, \ldots, N_x - 1$, $j = 2, \ldots, N_y - 1$). It can be calculated using the convected wave equation (1.5).
- The first time derivative of ϕ at t^n ($\dot{\phi}^n_I$) for the points in the left boundary ($i = 1$, $j = 2, \ldots, N_y - 1$), upper boundary ($i = 2, \ldots, N_x - 1$, $j = N_y$) and right boundary ($i = N_x$, $j = 2, \ldots, N_y - 1$). It can be computed imposing the non-reflecting boundary condition (1.21).
- The value of $\dot{\phi}^n_I$ for the points in the wake ($i = i_{te} + 1, \ldots, N_x$, $j = 1$), that can be obtained from the Kutta condition (1.8).
- For the corner points, the mean value of f^n_I in the boundary points next to them, i.e.:

$$f^n_{1,N_y} = \frac{1}{2}\left(f^n_{1,N_y-1} + f^n_{2,N_y}\right) \tag{2.1}$$

$$f^n_{N_x,N_y} = \frac{1}{2}\left(f^n_{N_x-1,N_y} + f^n_{N_x,N_y-1}\right) \tag{2.2}$$

- Zero for the rest of the points ($i = 1, \ldots, i_{te}$, $j = 1$). It is important to remark that this is just the value of $\dot{\phi}^n_I$ for the bottom points ahead the airfoil ($i = 1, \ldots, i_{le} - 1$, $j = 1$), because there the potential is always null, but not the value of any time derivative of ϕ in the airfoil ($i = i_{le}, \ldots, i_{te}$, $j = 1$).

All the values of f^n_I can be grouped into a column vector as well:

$$\mathbf{f}^n = \left[f^n_1, \ldots, f^n_{N_\phi}\right]^T$$

and it can be shown that $\mathbf{f}^n$ depends linearly on $\boldsymbol{\phi}^n$ and $\boldsymbol{\phi}^{n-1}$:

$$\mathbf{f}^n = \mathbf{A_0}\boldsymbol{\phi}^n + \mathbf{A_1}\boldsymbol{\phi}^{n-1} \tag{2.3}$$

where $\mathbf{A_0}$ and $\mathbf{A_1}$ are two constant sparse matrixes that are derived in subsection 2.2.2 by applying finite differences in the equations commented before.

Now suppose that $\boldsymbol{\phi}^{n-2}$ and $\boldsymbol{\phi}^{n-1}$ are known and $\boldsymbol{\phi}^n$ is unknown. At the inner points, where $f^n_I = \ddot{\phi}^n_I$, the following backward differentiation formula can be applied:

$$f^n_I = \frac{\phi^n_I - 2\phi^{n-1}_I + \phi^{n-2}_I}{\Delta t^2}; \quad I \in I_{inner} \tag{2.4}$$

whilst in the rest of points except the airfoil, where $f_I^n = \dot{\phi}_I^n$, it can be said that:

$$f_I^n = \frac{3\phi_I^n - 4\phi_I^{n-1} + \phi_I^{n-2}}{2\Delta t}; \quad I \in I_{bound} \tag{2.5}$$

At the points belonging to the airfoil, where f_I^n is not related to any of the derivatives of ϕ, the impenetrability boundary condition (1.6) is imposed. According to finite difference (1.15), the mentioned boundary condition can be written as:

$$w_p(t^n, x_i) = c_1\phi_{i,1}^n + c_2\phi_{i,2}^n + c_3\phi_{i,3}^n; \quad i = i_{le}, \ldots, i_{te}$$

with:

$$\begin{aligned}
c_1 &= -\frac{y_2 + y_3 - 2y_1}{(y_2 - y_1)(y_3 - y_1)} \\
c_2 &= \frac{y_3 - y_1}{(y_2 - y_1)(y_3 - y_2)} \\
c_3 &= -\frac{y_2 - y_1}{(y_3 - y_1)(y_3 - y_2)} \\
w_p(t^n, x_i) &= \left[\frac{\partial z_p(t,x)}{\partial t} + U_\infty \frac{\partial z_p(t,x)}{\partial x} - w_g(t,x)\right]_{x=x_i}^{t=t^n}
\end{aligned} \tag{2.6}$$

If the I index is used instead of the (i,j) pair, the latter equation becomes:

$$w_p(t^n, x_I) = c_1\phi_I^n + c_2\phi_{I+Nx}^n + c_3\phi_{I+2N_x}^n; \quad I \in I_{airfoil} \tag{2.7}$$

In the equations before, I_{inner}, I_{bound} and $I_{airfoil}$ are the sets of the I values at the inner points, the boundary points but the airfoil ones and the airfoil points, respectively.

For simplicity reasons, Einstein's summation criteria[1] is to be used from now. If relation (2.3) is substituted into (2.4)-(2.5) it follows:

$$\left[(\mathbf{A_0})_{IJ} - \frac{1}{\Delta t^2}\delta_{IJ}\right]\phi_J^n = \left[-(\mathbf{A_1})_{IJ} - \frac{2}{\Delta t^2}\delta_{IJ}\right]\phi_J^{n-1} + \frac{1}{\Delta t^2}\delta_{IJ}\phi_J^{n-2}; \; I \in I_{inner} \tag{2.8}$$

$$\left[(\mathbf{A_0})_{IJ} - \frac{3}{2\Delta t}\delta_{IJ}\right]\phi_J^n = \left[-(\mathbf{A_1})_{IJ} - \frac{2}{\Delta t}\delta_{IJ}\right]\phi_J^{n-1} + \frac{1}{2\Delta t}\delta_{IJ}\phi_J^{n-2}; \; I \in I_{bound} \tag{2.9}$$

where δ_{IJ} is the Kronecker tensor. Now, relations (2.7)-(2.9) provide a set of N_ϕ equations for N_ϕ unknowns, that are the components of $\boldsymbol{\phi}^n$. That set of equations can be written in the following matricial form:

$$\mathbf{B_0}\boldsymbol{\phi}^n = \mathbf{B_1}\boldsymbol{\phi}^{n-1} + \mathbf{B_2}\boldsymbol{\phi}^{n-2} + \mathbf{B_p}\mathbf{w_p^n} \tag{2.10}$$

where $\mathbf{w_p^n} = [w_p(t^n, x_{i_{le}}), \ldots, w_p(t^n, x_{i_{te}})]^T$ and where $\mathbf{B_0}$, $\mathbf{B_1}$, $\mathbf{B_2}$ and $\mathbf{B_p}$ are sparse

[1] Repeated index means summation along it.

matrixes that can be easily derived from equations (2.7)-(2.9):

$$(\mathbf{B_0})_{IJ} = \begin{cases} (\mathbf{A_0})_{IJ} - \frac{1}{\Delta t^2}\delta_{IJ} & ; I \in I_{inner} \\ (\mathbf{A_0})_{IJ} - \frac{3}{2\Delta t}\delta_{IJ} & ; I \in I_{bound} \\ c_1 & ; I \in I_{airfoil};\ J = I \\ c_2 & ; I \in I_{airfoil};\ J = I + N_x \\ c_3 & ; I \in I_{airfoil};\ J = I + 2N_x \\ 0 & ; \text{otherwise} \end{cases}$$

$$(\mathbf{B_1})_{IJ} = \begin{cases} -(\mathbf{A_1})_{IJ} - \frac{2}{\Delta t^2}\delta_{IJ} & ; I \in I_{inner} \\ -(\mathbf{A_1})_{IJ} - \frac{2}{\Delta t}\delta_{IJ} & ; I \in I_{bound} \\ 0 & ; \text{otherwise} \end{cases}$$

$$(\mathbf{B_2})_{IJ} = \begin{cases} \frac{1}{\Delta t^2}\delta_{IJ} & ; I \in I_{inner} \\ \frac{1}{2\Delta t}\delta_{IJ} & ; I \in I_{bound} \\ 0 & ; \text{otherwise} \end{cases}$$

$$(\mathbf{B_p})_{IJ} = \begin{cases} \delta_{IJ} & ; I \in I_{airfoil} \\ 0 & ; \text{otherwise} \end{cases}$$

Thus, the equation (2.10) is the one that allows calculating the values of the unknowns ϕ_I^n from the known values of ϕ_I^{n-1} and ϕ_I^{n-2}. It is important to point out that those unknowns, that are computed for the instant t^n, are obtained from their first and second time derivatives evaluated at t^n as well (see equations (2.4)-(2.5)), and not in t^{n-1}. Therefore, the explained scheme is implicit, which brings more numerical stability and permits bigger time step sizes.

Once the value of $\boldsymbol{\phi}^n$ is computed, it is possible to obtain the lift and the pitching moment over the airfoil using equations (1.9)-(1.10). For achieving this, the integrals that appear there can be computed by the trapezoid rule, and the time derivatives of ϕ in the airfoil can be approximated by $(\phi_I^n - \phi_I^{n-1})/\Delta t; I \in I_{airfoil}$ or by a higher order formula.

It has to be remarked that the matrixes $\mathbf{B_0}$,...,$\mathbf{B_p}$ can also be obtained in a more direct way —without the definition of $\mathbf{f}^n$— if the potential flow equations are discretized directly both in time and in space. However, they have been obtained here through the definition of $\mathbf{f}^n$ because the latter would make easier to use some other multistep methods in future developments instead of the BDF formulas used here.

2.2.2. Derivation of $\mathbf{A_0}$ and $\mathbf{A_1}$

As seen in the previous subsection, it is necessary to obtain the expressions of the matrixes $\mathbf{A_0}$ and $\mathbf{A_1}$ in order to implement the described marching time method. These matrixes can be obtained discretizing the potential theory equations with finite differences.

Inner points

Indeed, for the inner points, the discretized convected wave equation (1.5) reads as:

$$f_{ij}^n = \ddot{\phi}_{ij}^n = -2U_\infty \frac{\phi_{ij}^n - \phi_{i-1,j}^n - \phi_{i,j}^{n-1} + \phi_{i-1,j}^{n-1}}{\Delta t\,(x_i - x_{i-1})} +$$
$$\left(a_\infty^2 - U_\infty^2\right)\left(\alpha_i^1 \phi_{i+1,j}^n + \alpha_i^0 \phi_{i,j}^n + \alpha_i^{-1}\phi_{i-1,j}^n\right) + a_\infty^2 \left(\beta_j^1 \phi_{i,j+1}^n + \beta_j^0 \phi_{i,j}^n + \beta_j^{-1}\phi_{i,j-1}^n\right);$$
$$i = 2,\dots,N_x - 1, \quad j = 2,\dots,N_y - 1$$

where $\alpha_i^{-1}, \alpha_i^0, \alpha_i^1$ and $\beta_j^{-1}, \beta_j^0, \beta_j^1$ are coefficients given by (1.18):

$$\alpha_i^1 = \frac{2}{(x_{i+1}-x_i)(x_{i+1}-x_{i-1})}, \qquad \beta_j^1 = \frac{2}{(y_{j+1}-y_j)(y_{j+1}-y_{j-1})}$$
$$\alpha_i^0 = -\frac{2}{(x_{i+1}-x_i)(x_i-x_{i-1})}, \qquad \beta_j^0 = -\frac{2}{(y_{j+1}-y_j)(y_j-y_{j-1})}$$
$$\alpha_i^{-1} = \frac{2}{(x_i-x_{i-1})(x_{i+1}-x_{i-1})}, \qquad \beta_j^{-1} = \frac{2}{(y_j-y_{j-1})(y_{j+1}-y_{j-1})}$$

It is convenient to observe that an upwind finite difference has been used for the mixed second derivative ($\partial^2\phi/\partial t\partial x$), since the central formula would have resulted in an unstable scheme [11]. It also has to be pointed that a two-node formula has been employed for that upwind finite difference instead of a three-node one as proposed by the authors because, despite being less accurate, it results in a more stable scheme and the lack of accuracy is sufficiently compensated by the use of a non-uniform mesh.

Taking into account that, if I is the index corresponding to to the point denoted by (i,j), the indexes that correspond to the points just at the right $(i+1,j)$, left $(i-1,j)$, up $(i,j+1)$ and down $(i,j-1)$ are $I+1$, $I-1$, $I+N_x$ and $I-N_x$, respectively, the latter equation can be rewritten as:

$$f_I^n = (\mathbf{A_0})_{IJ}\,\phi_J^n + (\mathbf{A_1})_{IJ}\,\phi_J^{n-1}$$

with:

$$\begin{aligned}
(\mathbf{A_0})_{I,I} &= \frac{-2U_\infty}{\Delta t(x_I - x_{I-1})} + \left(a_\infty^2 - U_\infty^2\right)\alpha_I^0 + a_\infty^2\beta_I^0 \\
(\mathbf{A_0})_{I,I-1} &= \frac{2U_\infty}{\Delta t(x_I - x_{I-1})} + \left(a_\infty^2 - U_\infty^2\right)\alpha_I^{-1} \\
(\mathbf{A_0})_{I,I+1} &= \left(a_\infty^2 - U_\infty^2\right)\alpha_I^1 \\
(\mathbf{A_0})_{I,I-N_x} &= a_\infty^2\beta_I^{-1} \\
(\mathbf{A_0})_{I,I+N_x} &= a_\infty^2\beta_I^1 \\
(\mathbf{A_1})_{I,I} &= \frac{2U_\infty}{\Delta t(x_I - x_{I-1})} \\
(\mathbf{A_1})_{I,I-1} &= \frac{-2U_\infty}{\Delta t(x_I - x_{I-1})}
\end{aligned}$$

for $I \in I_{inner}$.

It has to be remarked that, in the expressions above and in the incoming ones, only the non-zero terms corresponding to the I-th row (for a given I) of the matrixes $\mathbf{A_0}$ and

$\mathbf{A_1}$ are shown. Thus, if the expression of a certain term $(\mathbf{A_0})_{I^*,J^*}$ (or $(\mathbf{A_1})_{I^*,J^*}$) is not found, that term will be null. On the other hand, an abuse of notation has been done (and will be done later again) and the different values of α_i^1, β_j^1, etc. have been denoted using the corresponding index I as α_I^1, β_I^1 and so on.

Left boundary

For the left boundary points, the discretized non-reflecting boundary condition 1.21 is:

$$f_{ij}^n = \dot{\phi}_{ij}^n = -\dot{R}_{ij}\left[\left(\alpha_i^0\phi_{i,j}^n + \alpha_i^1\phi_{i+1,j}^n + \alpha_i^2\phi_{i+2,j}^n\right)\cos\theta_{ij} + \left(\beta_j^1\phi_{i,j+1}^n + \beta_j^0\phi_{i,j}^n + \beta_j^{-1}\phi_{i,j-1}^n\right)\sin\theta_{ij} + \frac{\phi_{ij}^n}{2r_{ij}}\right]; \quad i=1, \quad j=2,\ldots,N_y-1$$

where $\dot{R}_{ij} = U_\infty\cos\theta_{ij} + \sqrt{a_\infty^2 - U_\infty^2\sin^2\theta_{ij}}$, r_{ij} and θ_{ij} are the polar coordinates of the (i,j) point as defined in section 1.5, and $\alpha_i^0, \alpha_i^1, \alpha_i^2, \beta_i^{-1}, \beta_i^0, \beta_i^1$ are coefficients given by (1.15) and (1.18):

$$\alpha_i^0 = -\frac{x_{i+1}+x_{i+2}-2x_i}{(x_{i+1}-x_i)(x_{i+2}-x_i)}, \qquad \beta_j^1 = \frac{y_j - y_{j-1}}{(y_{j+1}-y_j)(y_{j+1}-y_{j-1})}$$
$$\alpha_i^1 = \frac{x_{i+2}-x_i}{(x_{i+1}-x_i)(x_{i+2}-x_{i+1})}, \qquad \beta_j^0 = \frac{y_{j+1}-y_{j-1}}{(y_{j+1}-y_j)(y_j-y_{j-1})}$$
$$\alpha_i^2 = -\frac{x_{i+1}-x_i}{(x_{i+2}-x_i)(x_{i+2}-x_{i+1})}, \qquad \beta_j^{-1} = -\frac{y_{j+1}-y_j}{(y_j-y_{j-1})(y_{j+1}-y_{j-1})}$$

This gives more terms of the matrix $\mathbf{A_0}$:

$$\begin{aligned}
(\mathbf{A_0})_{I,I} &= -\dot{R}_I\left(\alpha_I^0\cos\theta_I + \beta_I^0\sin\theta_I + \frac{1}{2r_I}\right)\\
(\mathbf{A_0})_{I,I+1} &= -\dot{R}_I\alpha_I^1\cos\theta_I\\
(\mathbf{A_0})_{I,I+2} &= -\dot{R}_I\alpha_I^2\cos\theta_I\\
(\mathbf{A_0})_{I,I-N_x} &= -\dot{R}_I\beta_I^{-1}\sin\theta_I\\
(\mathbf{A_0})_{I,I+N_x} &= -\dot{R}_I\beta_I^1\sin\theta_I
\end{aligned}$$

for $I \in I_{left}$, where I_{left} represents the set of I values at the points in the left boundary (excluding the corners).

Upper boundary

Similarly, the discretized non-reflecting boundary condition for the upper boundary reads as:

$$f_{ij}^n = \dot{\phi}_{ij}^n = -\dot{R}_{ij}\left[\left(\alpha_i^{-1}\phi_{i-1,j}^n + \alpha_i^0\phi_{i,j}^n + \alpha_i^1\phi_{i+1,j}^n\right)\cos\theta_{ij} + \left(\beta_j^0\phi_{i,j}^n + \beta_j^{-1}\phi_{i,j-1}^n + \beta_j^{-2}\phi_{i,j-2}^n\right)\sin\theta_{ij} + \frac{\phi_{ij}^n}{2r_{ij}}\right]; \quad i=2,\ldots,N_x-1, \quad j=N_y$$

Now, $\alpha_i^{-1}, \alpha_i^0, \alpha_i^1, \beta_i^0, \beta_i^{-1}, \beta_i^{-2}$ are:

$$\alpha_i^1 = \frac{x_i - x_{i-1}}{(x_{i+1}-x_i)(x_{i+1}-x_{i-1})}, \qquad \beta_j^0 = \frac{2y_j - y_{j-1} - y_{j-2}}{(y_j - y_{j-1})(y_j - y_{j-2})}$$
$$\alpha_i^0 = \frac{x_{i+1} - x_{i-1}}{(x_{i+1}-x_i)(x_i-x_{i-1})}, \qquad \beta_j^{-1} = -\frac{y_j - y_{j-2}}{(y_j - y_{j-1})(y_{j-1} - y_{j-2})}$$
$$\alpha_i^{-1} = -\frac{x_{i+1} - x_i}{(x_i-x_{i-1})(x_{i+1}-x_{i-1})}, \qquad \beta_j^{-2} = \frac{y_j - y_{j-1}}{(y_j - y_{j-2})(y_{j-1} - y_{j-2})}$$

The corresponding terms of $\mathbf{A_0}$ are then:

$$\begin{aligned}
(\mathbf{A_0})_{I,I} &= -\dot{R}_I \left(\alpha_I^0 \cos\theta_I + \beta_I^0 \sin\theta_I + \frac{1}{2r_I} \right) \\
(\mathbf{A_0})_{I,I-1} &= -\dot{R}_I \alpha_I^{-1} \cos\theta_I \\
(\mathbf{A_0})_{I,I+1} &= -\dot{R}_I \alpha_I^{1} \cos\theta_I \\
(\mathbf{A_0})_{I,I-N_x} &= -\dot{R}_I \beta_I^{-1} \sin\theta_I \\
(\mathbf{A_0})_{I,I-2N_x} &= -\dot{R}_I \beta_I^{-2} \sin\theta_I
\end{aligned}$$

for $I \in I_{upper}$, being I_{upper} the set of values that I takes at the points in the upper boundary (excluding the corners as well).

Right boundary

The same procedure can be applied for the right boundary. Now, the corresponding discretized equation is:

$$\begin{aligned}
f_{ij}^n = \dot{\phi}_{ij}^n = -\dot{R}_{ij} \Big[&\left(\alpha_i^{-2}\phi_{i-2,j}^n + \alpha_i^{-1}\phi_{i-1,j}^n + \alpha_i^0\phi_{i,j}^n\right)\cos\theta_{ij} + \\
&\left(\beta_j^1\phi_{i,j+1}^n + \beta_j^0\phi_{i,j}^n + \beta_j^{-1}\phi_{i,j-1}^n\right)\sin\theta_{ij} + \frac{\phi_{ij}^n}{2r_{ij}}\Big]; \quad i = N_x, \quad j = 2, \dots, N_y - 1
\end{aligned}$$

with:

$$\alpha_i^0 = \frac{2x_i - x_{i-1} - x_{i-2}}{(x_i - x_{i-1})\,(x_i - x_{i-2})}, \qquad \beta_j^1 = \frac{y_j - y_{j-1}}{(y_{j+1} - y_j)(y_{j+1} - y_{j-1})}$$
$$\alpha_i^{-1} = -\frac{x_i - x_{i-2}}{(x_i - x_{i-1})\,(x_{i-1} - x_{i-2})}, \qquad \beta_j^0 = \frac{y_{j+1} - y_{j-1}}{(y_{j+1} - y_j)(y_j - y_{j-1})}$$
$$\alpha_i^{-2} = \frac{x_i - x_{i-1}}{(x_i - x_{i-2})\,(x_{i-1} - x_{i-2})}, \qquad \beta_j^{-1} = -\frac{y_{j+1} - y_j}{(y_j - y_{j-1})(y_{j+1} - y_{j-1})}$$

that leads to:

$$\begin{aligned}
(\mathbf{A_0})_{I,I} &= -\dot{R}_I \left(\alpha_I^0 \cos\theta_I + \beta_I^0 \sin\theta_I + \frac{1}{2r_I} \right) \\
(\mathbf{A_0})_{I,I-1} &= -\dot{R}_I \alpha_I^{-1} \cos\theta_I \\
(\mathbf{A_0})_{I,I-2} &= -\dot{R}_I \alpha_I^{-2} \cos\theta_I \\
(\mathbf{A_0})_{I,I-N_x} &= -\dot{R}_I \beta_I^{-1} \sin\theta_I \\
(\mathbf{A_0})_{I,I+N_x} &= -\dot{R}_I \beta_I^{1} \sin\theta_I
\end{aligned}$$

for $I \in I_{right}$, where I_{right} is the set of I values at the points in the right boundary (excluding the corners).

Corners

For the upper-left and upper-right corner points, f_I^n is equal to its mean value in the two adjacent points, as indicated by equations (2.1)-(2.2). Those two relations can be rewritten as:

$$
\begin{aligned}
f_I^n &= \frac{1}{2}\left(f_{I-N_x} + f_{I+1}\right), && I = (N_y - 1)N_x + 1 \\
f_I^n &= \frac{1}{2}\left(f_{I-1} + f_{I-N_x}\right), && I = N_x N_y = N_\phi
\end{aligned}
$$

Using now equation (2.3) and taking into account that $(\mathbf{A_1})_{IJ} = 0$ when I does not belong to an inner point, it follows that:

$$
\begin{aligned}
(\mathbf{A_0})_{IJ} &= \frac{1}{2}\left[(\mathbf{A_0})_{I-N_x,J} + (\mathbf{A_0})_{I+1,J}\right], && I = (N_y - 1)N_x + 1, && J = 1, \ldots, N_\phi \\
(\mathbf{A_0})_{IJ} &= \frac{1}{2}\left[(\mathbf{A_0})_{I-1,J} + (\mathbf{A_0})_{I-N_x,J}\right], && I = N_\phi, && J = 1, \ldots, N_\phi
\end{aligned}
$$

Wake

Finally, the discretized Kutta condition (1.8), that applies to the wake, reads as:

$$
f_{ij}^n = \dot{\phi}_{ij}^n = -U_\infty \frac{\phi_{ij}^n - \phi_{i-1,j}^n}{x_i - x_{i-1}}
$$

Here, upwinding is used again in order to make the scheme stable. Naming I_{wake} to the set of values that I takes at the wake points, the latter equation leads to:

$$
\begin{aligned}
(\mathbf{A_0})_{I,I} &= \frac{-U_\infty}{x_I - x_{I-1}} \\
(\mathbf{A_0})_{I,I-1} &= \frac{U_\infty}{x_I - x_{I-1}}
\end{aligned}
$$

for $I \in I_{wake}$.

2.2.3. Efficient scheme implementation. Summary of all the steps

Once $\mathbf{A_0}$ and $\mathbf{A_1}$ have been derived, it is possible to compute the matrixes that appear in equation (2.10) and implement then the modified Hariharan-Ping-Scott method. However, since the system given by the mentioned equation has to be solved for every simulated instant t^n, some ideas are to be commented first in order to achieve a more efficient resolution.

For simplicity reasons, let the equation (2.10) be written as:

$$
\mathbf{B_0}\boldsymbol{\phi}^n = \mathbf{b}^n \tag{2.11}
$$

where $\mathbf{b}^n = \mathbf{B_1}\boldsymbol{\phi}^{n-1} + \mathbf{B_2}\boldsymbol{\phi}^{n-2} + \mathbf{B_p}\mathbf{w_p^n}$. Although $\mathbf{b}^n$ is different at every simulated instant, the matrix $\mathbf{B_0}$ of the system is always the same. Therefore, the computational cost can be greatly reduced if a LU decomposition is done at the beginning and then, for every t^n, the solution of the system is found by solving the two associated triangular systems instead of using a direct resolution method.

As $\mathbf{B_0}$ is a sparse matrix, the LU factorization is performed much faster and the resultant matrixes are much sparser if rows and column permutations are permitted [17], i.e.:

$$\mathbf{PB_0Q} = \mathbf{LU}$$

where $\mathbf{P}$, $\mathbf{Q}$ are permutation matrixes, and $\mathbf{L}$, $\mathbf{U}$ are the usual lower and upper triangular matrixes.

In order to solve the system given by $\mathbf{B_0}\boldsymbol{\phi}^n = \mathbf{b}^n$ with the latter factorization, let $\hat{\boldsymbol{\phi}}^n$ be a vector (say *permuted vector of potentials*) that verifies $\boldsymbol{\phi}^n = \mathbf{Q}\hat{\boldsymbol{\phi}}^n$. In that case, premultiplying equation (2.11) by $\mathbf{P}$ it follows that:

$$\underbrace{\mathbf{PB_0Q}}_{=\mathbf{LU}}\hat{\boldsymbol{\phi}}^n = \mathbf{Pb}^n$$

Hence, $\hat{\boldsymbol{\phi}}^n$ can be computed by solving two triangular systems:

$$\hat{\boldsymbol{\phi}}^n = \mathbf{U}\backslash\left(\mathbf{L}\backslash\left(\mathbf{Pb}^n\right)\right) \tag{2.12}$$

and then:

$$\boldsymbol{\phi}^n = \mathbf{Q}\left(\mathbf{U}\backslash\left(\mathbf{L}\backslash\left(\mathbf{Pb}^n\right)\right)\right) \tag{2.13}$$

In the equations before, the notation $\mathbf{x} = \mathbf{A}\backslash\mathbf{b}$ indicates that $\mathbf{x}$ has to be obtained by solving the system $\mathbf{Ax} = \mathbf{b}$ with an appropiate method, and not by inverting the matrix of the system (which would be denoted by $\mathbf{x} = \mathbf{A}^{-1}\mathbf{b}$)[2]. In the present case, since the matrixes of the systems are $\mathbf{L}$ and $\mathbf{U}$, forward and backward substitution techniques can be used, as well as any iterative method suitable for lower and upper sparse matrixes.

A possible approach for the method would be to calculate the potential $\boldsymbol{\phi}^n$ for every instant using equation (2.13). However, comparing that equation with (2.12), it can be seen that computing $\hat{\boldsymbol{\phi}}^n$ instead is slightly more efficient because a permutation is saved at every t^n. For that reason, the scheme presented here relies in calculating the permuted vector of potentials instead of the original one.

Considering that, if the relation $\boldsymbol{\phi}^n = \mathbf{Q}\hat{\boldsymbol{\phi}}^n$ and the expression of $\mathbf{b}^n$ are substituted in (2.12), the final equation for the marching time method reads as:

$$\hat{\boldsymbol{\phi}}^n = \mathbf{U}\backslash\left(\mathbf{L}\backslash\left(\hat{\mathbf{B_1}}\hat{\boldsymbol{\phi}}^{n-1} + \hat{\mathbf{B_2}}\hat{\boldsymbol{\phi}}^{n-2} + \hat{\mathbf{B_p}}\mathbf{w_p^n}\right)\right) \tag{2.14}$$

where $\hat{\mathbf{B_1}} = \mathbf{PB_1Q}$, $\hat{\mathbf{B_2}} = \mathbf{PB_2Q}$ and $\hat{\mathbf{B_p}} = \mathbf{PB_p}$.

The whole scheme can be summarized in the following steps:

- Input data: $w_p(t,x)$, x_i, y_j, ρ_∞, U_∞, a_∞, c, Δt and t_f (final simulation time).
- Compute matrixes $\mathbf{A_0}$ and $\mathbf{A_1}$ as shown in section 2.2.2. Then, calculate matrixes $\mathbf{B_0}$, $\mathbf{B_1}$, $\mathbf{B_2}$ and $\mathbf{B_p}$ as pointed in section 2.2.
- Perform the LU factorization of $\mathbf{B_0}$ with rows and columns permutations.

[2]This notation is clearly inspired in the corresponding Matlab command.

- Permute $\mathbf{B_1}$, $\mathbf{B_2}$ and $\mathbf{B_p}$ to obtain $\hat{\mathbf{B_1}}$, $\hat{\mathbf{B_2}}$ and $\hat{\mathbf{B_p}}$ as indicated just after equation (2.14).

- Assume $t^n = 0$ and $\hat{\boldsymbol{\phi}}^{n-2} = \hat{\boldsymbol{\phi}}^{n-1} = \mathbf{0}$.

- While $t^n \leq t_f$:

  - Compute $\hat{\boldsymbol{\phi}}^n$ using equation (2.14).
  - Extract the values of ϕ^n in the airfoil from $\hat{\boldsymbol{\phi}}^n$ and apply the trapezoid rule in equations (1.9)-(1.10) to obtain the lift l^n and the pitching moment m^n by length unit at t^n.
  - Actualize variables:

$$\hat{\boldsymbol{\phi}}^{n-2} \leftarrow \hat{\boldsymbol{\phi}}^{n-1}, \quad \hat{\boldsymbol{\phi}}^{n-1} \leftarrow \hat{\boldsymbol{\phi}}^{n}, \quad t^n = t^n + \Delta t$$

2.3. Results

In order to validate the method, the lift and the pitching moment coefficients, denoted by c_l and c_m respectively, are to be calculated as a funtion of the adimensional time $U_\infty t/c$ for three typical problems in unsteady aerodynamics:

- Wagner's problem or response to a sudden change of the angle of attack.

- Theodorsen's problem or response to an harmonic motion of the airfoil.

- Küssner's problem or response to a step gust.

The pitching moment coefficient is measured over the leading edge and is positive nose down. As usual, both coefficients can be obtained from the lift and the moment over the leading edge through the following relations:

$$c_l = \frac{l}{\frac{1}{2}\rho_\infty U_\infty^2 c}, \quad c_m = \frac{m_{le}}{\frac{1}{2}\rho_\infty U_\infty^2 c^2}$$

The obtained results have been compared with other ones calculated with the Hernandes-Soviero method [6][12][13] (about which some commentaries were made in the introductory chapter of this text) and, in some cases, with other theoretical ones as well provided by Wagner [9], Theodorsen [21], Küssner [14] and Mateescu [16].

In the three cases, the domain was the rectangle inside the straight lines $x = -10c$, $x = 10c$, $y = 0$ and $y = 10c$ (with $c = 2$, although the dimensionless results do not depend on c). The grid consisted in 151×151 points, with more points near the airfoil because the latter is the source of all the waves and therefore the gradient of ϕ is higher there. In particular,

$$
\begin{aligned}
x_i &= \begin{cases} -10c + 10c\sin\left(\dfrac{i-1}{50}\dfrac{\pi}{2}\right), & i = 1,\ldots,50 \\[2ex] \dfrac{c}{50}(i-51), & i = 51,\ldots,101 \\[2ex] 10c - 9c\cos\left(\dfrac{i-101}{50}\dfrac{\pi}{2}\right), & i = 102,\ldots,151 \end{cases} \\
y_j &= 10c - 10c\cos\left(\frac{j-1}{150}\frac{\pi}{2}\right), \qquad j = 1,\ldots,151
\end{aligned}
$$

which results in the mesh shown in figure 2.2.

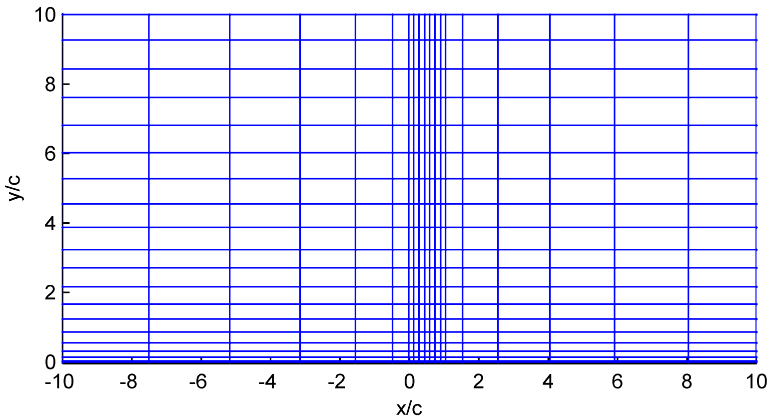

Figure 2.2: Mesh used in this work. Observe that it has been refined near the airfoil, which is the segment $0 \leq x/c \leq 1$, $y = 0$. For a better visualization, only 2 every 15 lines have been represented.

2.3.1. Wagner's problem

Consider an airfoil whose angle of attack is 0 at $t = 0^-$ and $\Delta\alpha$ at $t \geq 0^+$. There are not any kind of gusts ($w_g = 0$). For $t > 0$, it can be said that the induced velocities over the airfoil are:

$$w_p(t,x) = \frac{\partial z_p}{\partial t} + U_\infty \frac{\partial z_p}{\partial x} = -U_\infty \Delta\alpha, \quad t > 0$$

In this case, $\Delta\alpha$ has taken to be 1. The results for any other $\Delta\alpha$ will be proportional, as the problem is linear.

The results obtained for the lift and the pitching moment coefficients with the adapted Hariharan-Ping-Scott method for different values of the upstream Mach number M_∞ are plotted in figure 2.3. The theoretical Wagner's solution (valid for $M_\infty = 0$) and the results obtained with the Hernandes-Soviero method are represented as well. As seen in that figure, both numerical methods give the same lift coefficient, even for $t = 0$, and show similar values for c_m, existing only a slight discrepancy in the c_m at the first instants. Both methods converge to the Wagner's solution as $M_\infty = 0$, as expected, although the vortex-lattice does it with slightly better accuracy.

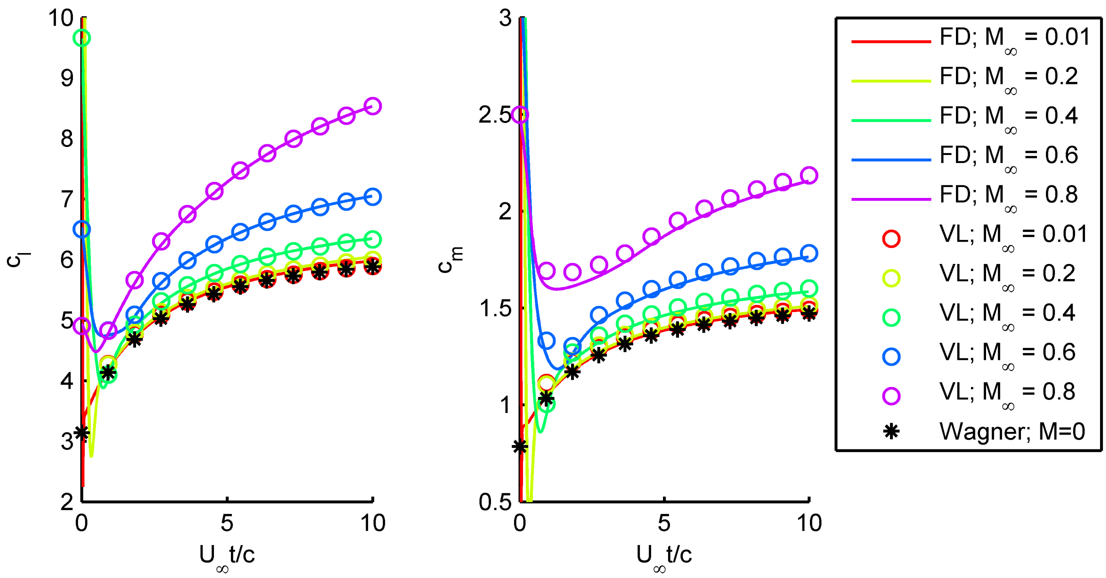

Figure 2.3: Lift and pitching moment coefficient obtained with the adapted Hariharan-Ping-Scott's finite difference method (FD) and with the Hernandes-Soviero's vortex-lattice method (VL) for the Wagner's problem. The Wagner's solution, valid for $M_\infty = 0$, is also represented.

It is important to point out that there seems to be a discrepancy in $t = 0$ between the numerical methods and the Wagner's solution, because the firsts present a peak at that instant and the latter tends to a finite number (see figure 2.4). However, it is shown in reference [6] that, if incompressibility is assumed, there has to be a peak (from a theoretical point of view) at $t = 0$, but that peak is not usually taken into account in the literature when explaining the Wagner's solution. Hence, the discrepancy at $t = 0$ is justified.

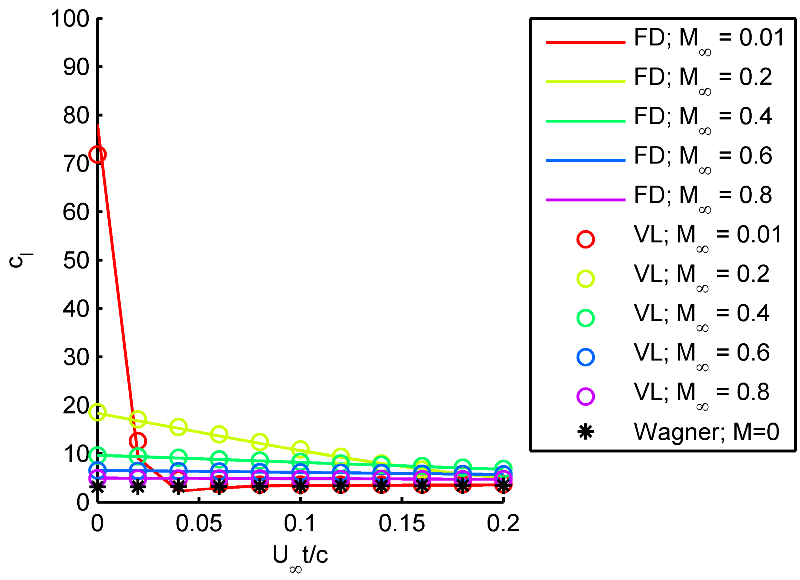

Figure 2.4: Numerical and theoretical solutions for the lift coefficient near $t = 0$. For the numerical solutions, the lower M_∞ is, the greater the value of c_l is. However, the theoretical solution for $M_\infty = 0$ does not tend to infinity at $t = 0$.

2.3.2. Theodorsen's problem

Now consider a rigid flat airfoil defined by three parameters: the x-coordinate of a point called elastic axis (say x_e), the vertical displacement h of this point (positive downwards) and the rotation α around it (positive nose up), as shown in figure 2.5.

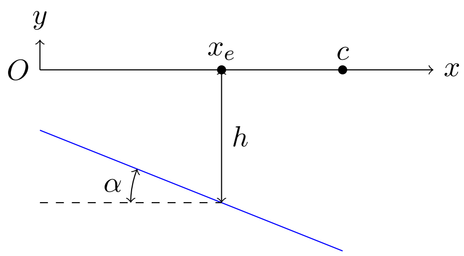

Figure 2.5: Degrees of freedom that describe the harmonic motion of a rigid airfoil.

In a harmonic motion, any variable $\psi(t)$ can be written as $\psi(t) = \Re\left(\tilde{\psi}e^{j\omega t}\right)$, where j is the complex unit, ω is the angular frequency of the motion and $\tilde{\psi}$ is a complex number called phasor. Using this notation and deducing the relation between $z_p(t, x)$, $h(t)$, $\alpha(t)$ and x_e, it can be shown that the phasor $\tilde{w_p}$ of the induced velocities over the airfoil w_p reads as:

$$\tilde{w_p}(x) = -j\omega\tilde{h} - \jmath\omega\tilde{\alpha}(x - x_e) - U_\infty\tilde{\alpha}$$

and therefore:

$$w_p(t, x) = \Re\left[\left(-j\omega\tilde{h} - \jmath\omega\tilde{\alpha}(x - x_e) - U_\infty\tilde{\alpha}\right) e^{j\omega t}\right]$$

For the present case, the following values have been considered:

$$x_e = 0.75c, \quad \tilde{h} = 0.05c, \quad \tilde{\alpha} = (3+4j)\frac{\pi}{180}, \quad \frac{\omega c}{U_\infty} = 0.16$$

The obtained results are represented in figure 2.6, where they are also compared with theoretical solutions provided by Theodorsen [21] and Mateescu [16] and, as well, with numerical results calculated with the Hernandes-Soviero method. As can be seen, the agreement between all the solutions is very good, both for the lift and the pitching moment.

Also, as an example to show how the waves propagate, the potential ϕ has been plotted in figure 2.7 as a function of x and y for a given instant and Mach number. In that figure, it can be appreciated that the waves are originated first in the airfoil as a consequence of its motion and, then, they propagate and dissipate among the space with a non-cylindrical symmetry, convecting with the upstream velocity along the $x-axis$.

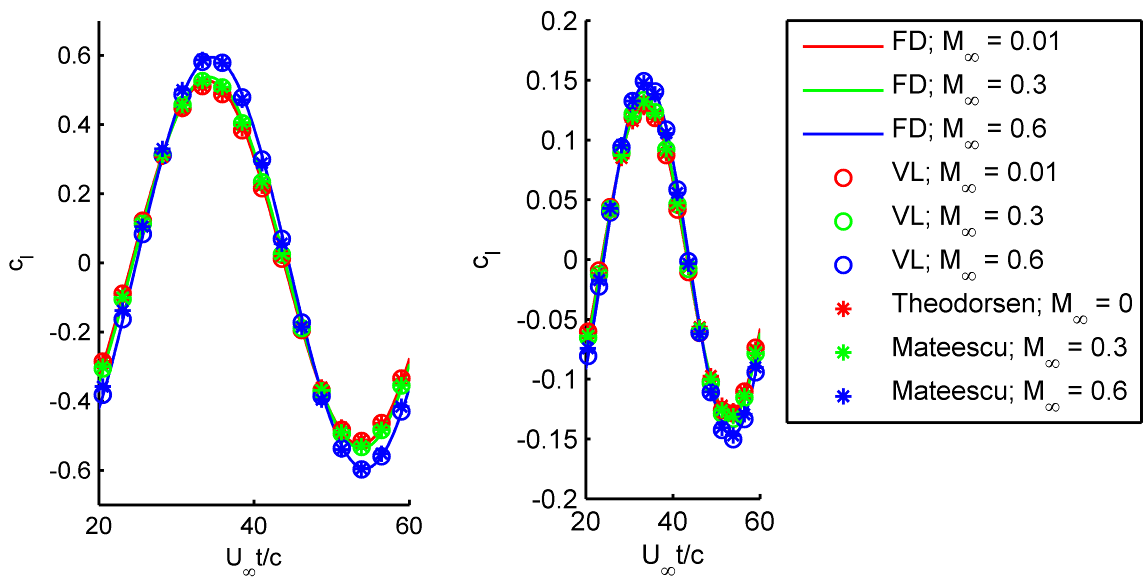

Figure 2.6: Lift and pitching moment coefficient in an harmonic motion.

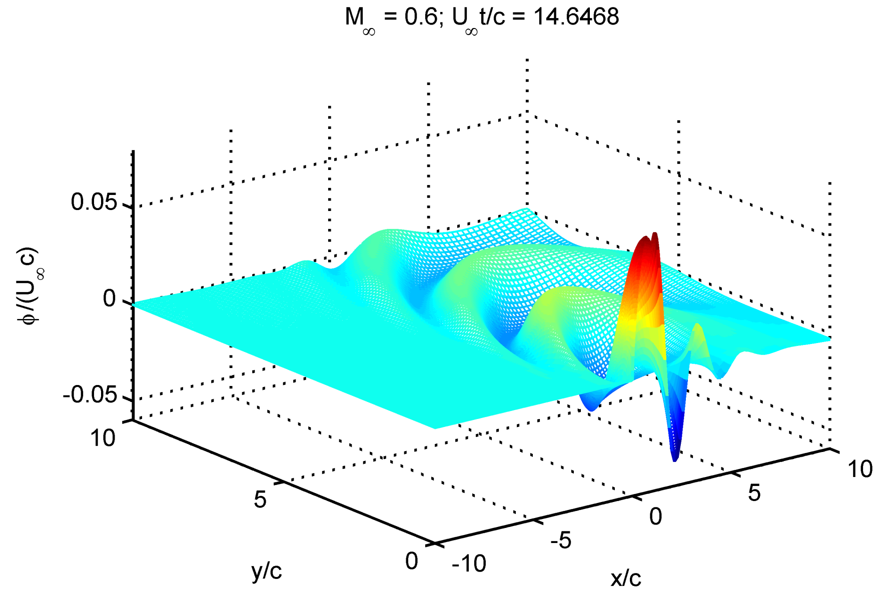

(a) $x - y - \phi$ view

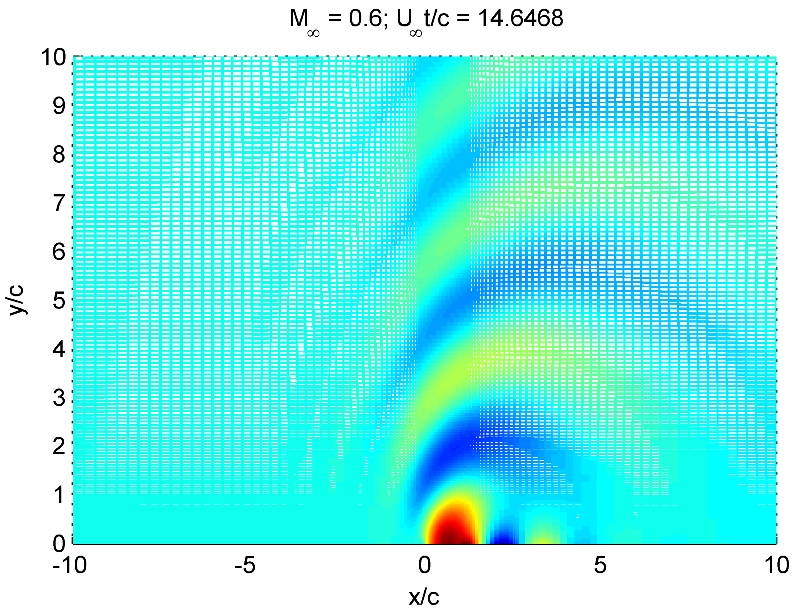

(b) $x - y$ view

Figure 2.7: Wave propagation for a harmonic motion of the airfoil. For this example, $\tilde{\alpha}$ has been set to 0 and the non-dimensional frequency $\omega c/U_\infty$ to 3. Compare this image with figure 1.4.

2.3.3. Küssner's problem

Finally, consider an airfoil flying at speed U_∞ that enters a sharped-edge vertical gust, as shown in figure 2.8. Assuming that the airfoil keeps flying horizontally after entering in the gust, the induced velocities on the airfoil are, according to relation (2.6):

$$w_p(t,x) = -w_g(t,x) = -w_0\sigma\left(t - \frac{x}{U_\infty}\right)$$

where $\sigma(t)$ is the Heaviside or step function.

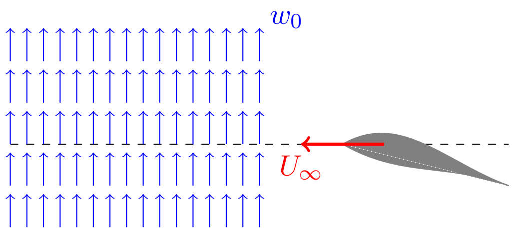

Figure 2.8: Scheme of an airfoil flying at velocity U_∞ that enters in a vertical step-like gust of speed w_0. The airfoil is assumed to keep flying horizontally.

The lift coefficient obtained for $w_0 = U_\infty$ both by the finite differences method and by the vortex-lattice one is shown in figure 2.9. Again, the results present very good agreement and converge to Küssner's solution [14] when M_∞ is small. However, the results provided by the modified Hariharan-Ping-Scott method present some noise for $M_\infty \simeq 0$ from $t = 0$ to $t = c/U_\infty$, i.e., when the airfoil has not fully entered in the gust and therefore w_p is discontinuous at some point in the airfoil. With the Hernandes-Soviero method, that noise is avoided by choosing a time step Δt which makes that discontinuity to advance an integer number of grid points along the airfoil every simulated instant. Unluckily, that criteria does not work for the finite difference method and noise still appears at the first instants. Nevertheless, the sharp-edge gust is just an ideal case and more realistic models, such as the hyperbolic-tangent-like or sinusoidal gusts, could provide smoother results.

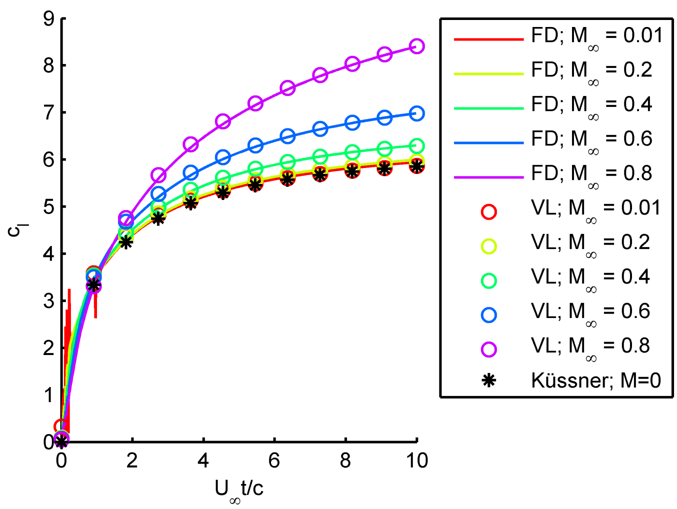

Figure 2.9: Evolution of the lift coefficient after a sharp-edge gust.

2.4. Convergence and stability comparison between the modified and the original Hariharan-Ping-Scott methods

The aim of this section is to show the positive effect of the improvements proposed here for the original Hariharan-Ping-Scott method, i.e., the use of a non-uniform mesh and an implicit time integration scheme.

On one hand, figure 2.10 shows the influence of the grid by presenting the lift coefficient for the Wagner's problem (with $M_\infty = 0.05 \simeq 0$) obtained with: (i) the non-uniform mesh used in previous results, (ii) an uniform mesh of 201×151 points for the same domain $[-10c, 10c] \times [0, 10c]$ (say big domain) and (iii) an uniform mesh of 151×151 points for a smaller domain $[-3c, 3c] \times [0, 6c]$ (say small domain). In all cases, Δt has been set to $c/U_\infty/200$, the grid was chosen to have nodes just at the leading and trailing edges and the previously-explained implicit time integration scheme was used. As can be seen, the non-uniform mesh give results that converge clearly faster to the theoretical Wagner's solution. At the same time, the uniform mesh and the big domain provide a solution that seems to be proportional to Wagner's, whereas the uniform mesh and the small domain give the worst results.

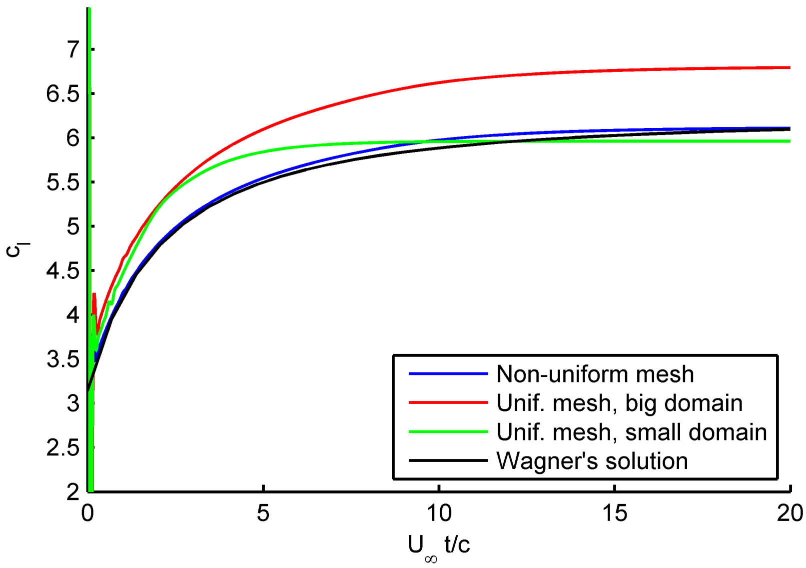

Figure 2.10: Comparison of the evolution of the lift coefficient for different meshes.

This happens because the non-uniform mesh concentrates more points in the airfoil (which is the focus of the waves and therefore the gradient of ϕ is higher there (see figure 2.7)) and also occupies a big enough region to simulate an infinite domain. With an uniform mesh, it is very difficult to satisfy both facts at the same time unless a big and very dense grid is used, leading in that case to memory and slowness problems.

On the other hand, figure 2.11 displays the effect of making the algorithm implicit. There, the lift coefficient for the Wagner's problem is plotted for different values of Δt and (i) the non-uniform mesh used in previous results and implicit scheme, (ii) an uniform mesh and implicit scheme and (iii) an uniform mesh and explicit scheme. In all cases, the domain was the same ($[-10c, 10c] \times [0, 10c]$). As can be seen, the explicit algorithm can become unstable even for much smaller time steps than the used for the implicit algorithm. Also, the solutions present less noise when using the implicit schemes.

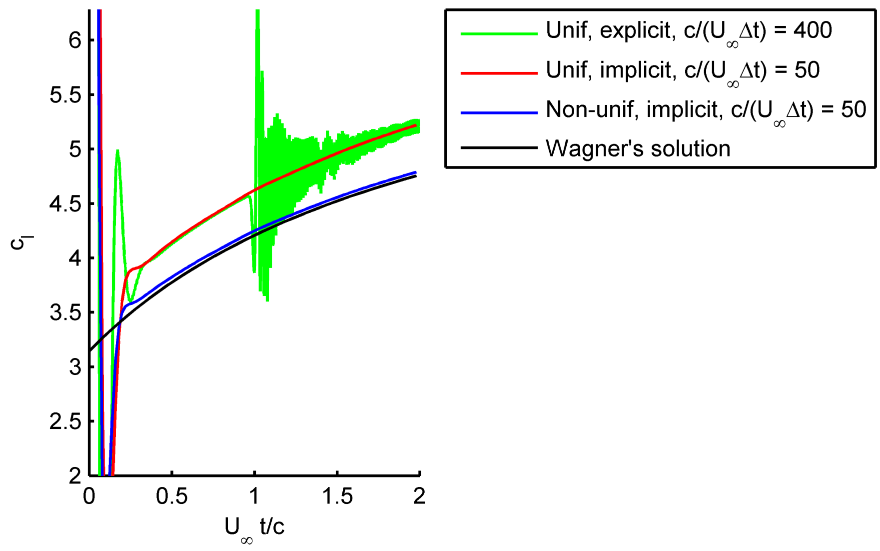

(a)

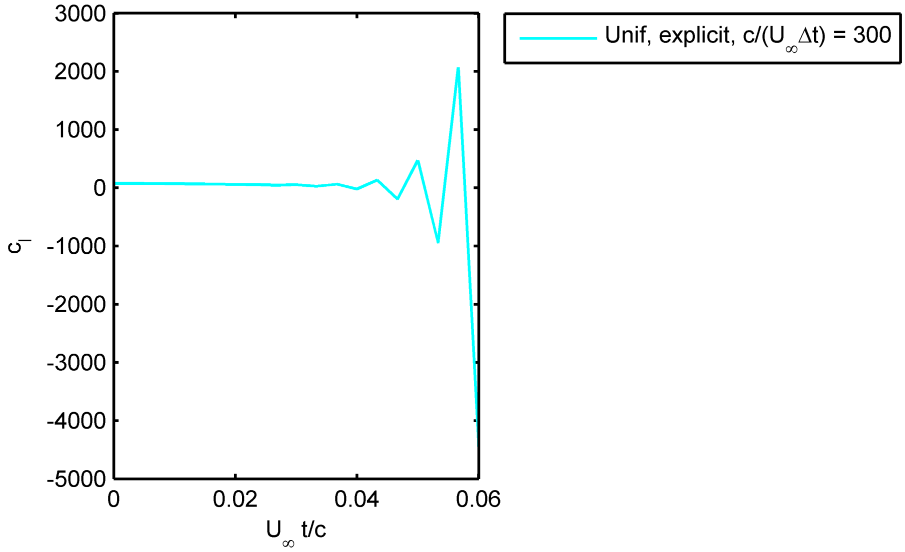

(b)

Figure 2.11: Evolution of the lift coefficient for implicit and explicit schemes and stable (a) and unstable (b) solutions.

Finally, it is important to point that all the above results have been obtained with algorithms that employ a two-node formula for approximating the term $\partial\phi/\partial x$ at the inner points (see section 2.2.2), instead of the three-node formula proposed originally by the authors. Since a two-node formula is less accurate than a three-node one, it is possible to wonder if the discrepancies shown before are caused by its use and not just because the mesh is uniform or the domain is not big enough. To clarify this point, the lift coefficient obtained with an uniform mesh, an explicit scheme and the two-node formula is compared in figure 2.12 with the one obtained with an uniform mesh, an explicit scheme and the three-node formula (i.e., the truly original Hariharan-Ping-Scott method). As can be seen there, both provide the same results, thus, all the above shown discrepancies are due to the use of an uniform mesh, a not big enough domain, etc. and never due to the use of a two-node formula.

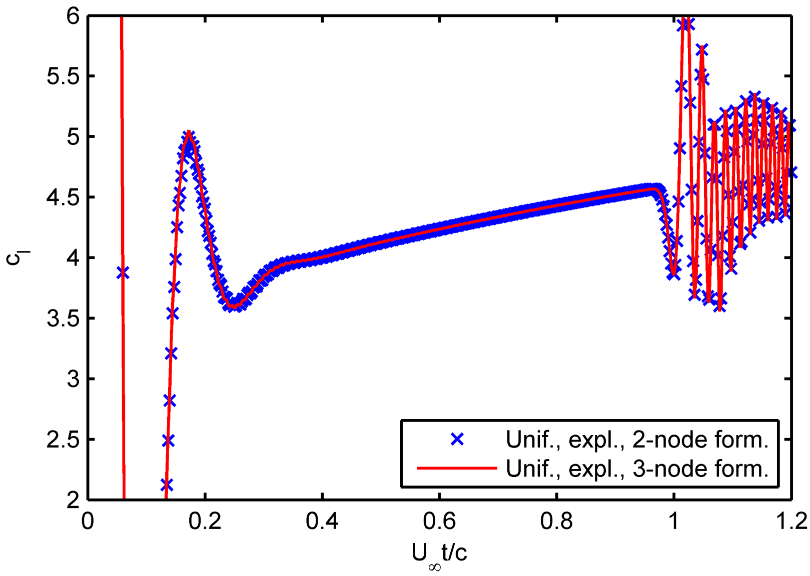

Figure 2.12: Evolution of the lift coefficient when using the two-node or the three-node formula. Δt has been set to $c/U_\infty/400$ in both cases. The absolute error has been calculated and is of the order of 0.01.

2.5. Convergence and efficiency comparison between the modified Hariharan-Ping-Scott and the modified Hernandes-Soviero methods

In this section, the effect of Δt in the convergence to the final result and in the total run time (until an instant t^n) is to be studied for the modified Hariharan-Ping-Scott and the modified Hernandes-Soviero methods. For the latter, the saving-time truncation algorithm presented in reference [6] has been used.

First, a harmonic motion has been imposed to the airfoil and the root mean square (RMS) of c_l has been computed. The period T has been chosen to be $0.5\,c/U_\infty$, i.e., of the same order of the residence time of the flow particles past the airfoil, and the upstream Mach number was set to 0.5. The results, plotted in figure 2.13(a), show that both methods converge with the same speed to the final value as Δt becomes smaller. Also, it can be seen that the absolute error between the two methods is 0.05 which, compared with the RMS value ($\simeq 3.45$), gives a relative error of 1.45%. On the other hand, the figure 2.13(b) shows the relative error between the RMS obtained for a generic Δt and the final RMS (obtained for the smallest Δt). As can be seen, for a time step 200 times lower than the characteristic time c/U_∞, the relative error is almost 0.1% for the two methods. Thus, for low-medium frequencies, that could be a recommended time step size for achieving good results.

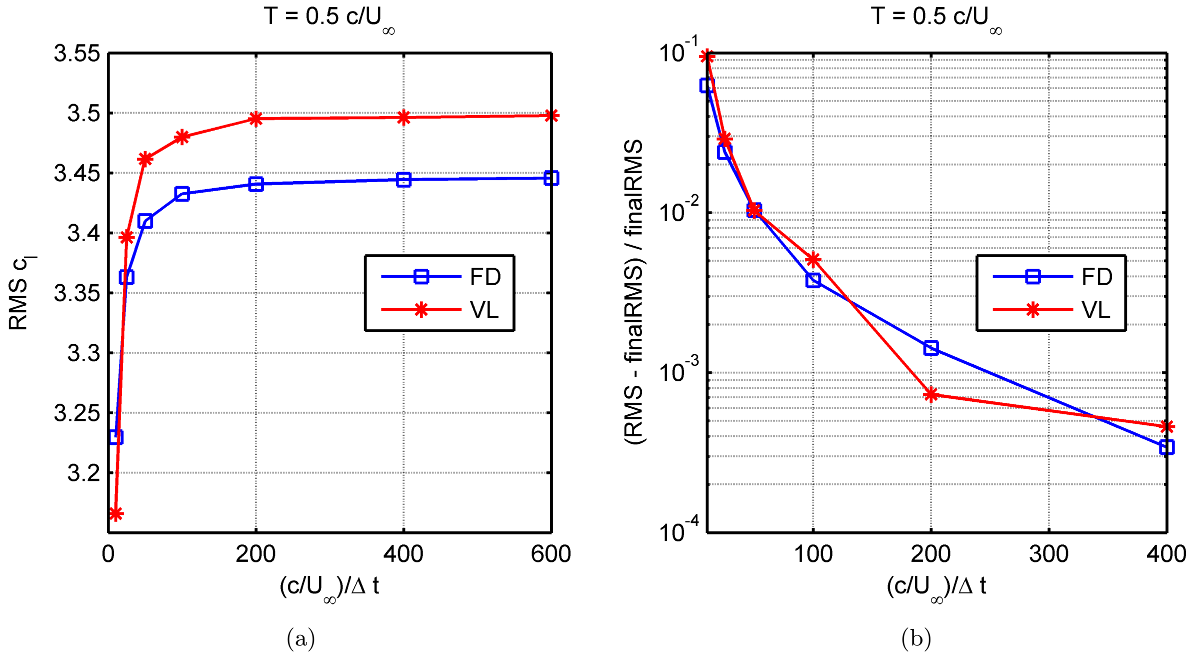

Figure 2.13: Effect of Δt in the convergence of the results for a medium-frequency harmonic motion.

The same has been done for a high-frequency motion. In this case, the period has been chosen to be $0.05c/U_\infty$, and the results have been plotted in figures 2.14(a)-(b). The behaviour is the same that the shown for a low-medium frequency movement with the exception that, now, Δt has to be 50 times smaller that the period of the movement to achieve 0.1% of accuracy respect the final value of RMS.

Finally, the total run time spent in solving the low-frequency-motion problem has been plotted in figure 2.15 as a function of the simulated time t^n for different values of Δt. The following aspects can be appreciated there:

- For the finite differences method, the run time increases linearly with the simulated time t^n. This is due to the fact that, for every instant, the main run time is employed in solving the two triangular systems associated to the equation (2.14). Since the column vector $\hat{\mathbf{b}}^n = \hat{\mathbf{B}}_\mathbf{1}\hat{\boldsymbol{\phi}}^{n-1} + \hat{\mathbf{B}}_\mathbf{2}\hat{\boldsymbol{\phi}}^{n-2} + \hat{\mathbf{B}}_\mathbf{p}\mathbf{w}_\mathbf{p}^\mathbf{n}$ should always take more or less the same time to be calculated, those systems should also take more or less the same time to be solved for every instant t^n.
- The run time for the vortex-lattice method increases parabolically at the beginning, and linearly from certain instant (say t^*). As pointed in reference [6], this happens

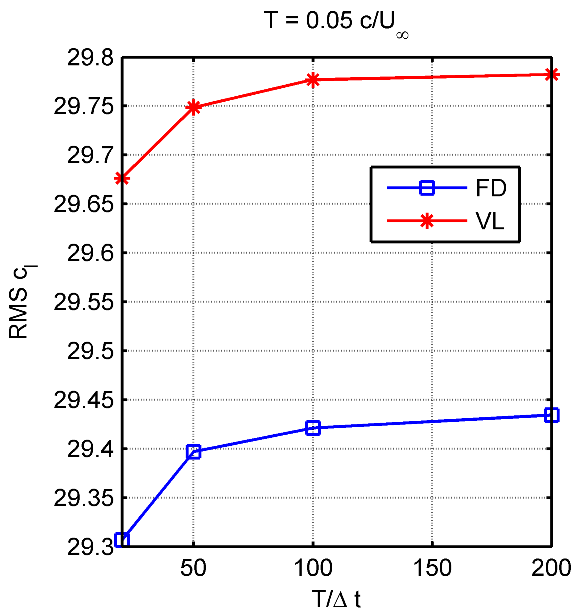

(a)

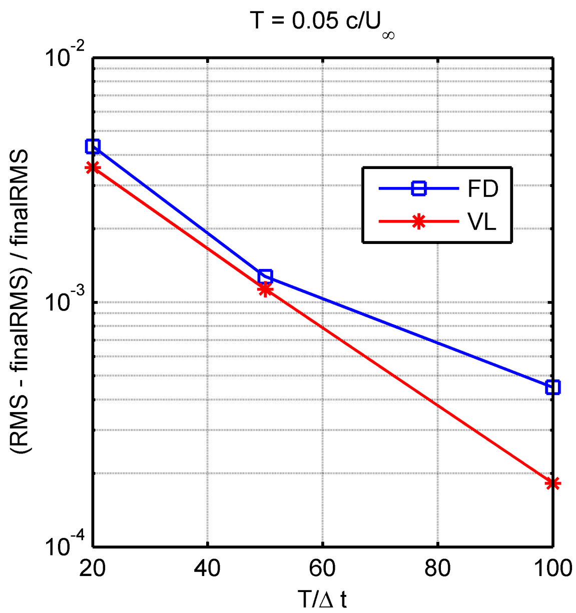

(b)

Figure 2.14: Effect of Δt in the convergence of the results for a high-frequency harmonic motion.

because a system of the kind $\mathbf{A}\mathbf{x}^n = \mathbf{b}'^n$ has to be solved every instant t^n. However, the main run time is not employed here to solve that system, but to calculate the term $\mathbf{b}'^n$. Since this term depends on the whole history before (when $t^n < t^*$), it becomes increasingly expensive to compute as the simulation time passes by. Arrived at t^*, the truncation method proposed in [6] starts working and it is not necessary to calculate $\mathbf{b}'^n$ from the whole history before, but from a non-increasing 'recent' history and an approximation of the 'old' one, making the computational cost to stop being increasingly expensive.

- For low final simulation times or big time step sizes the modified Hernandes-Soviero method is faster than the modified Hariharan-Ping-Scott one. This is due to the fact that, in the vortex-lattice method, the only unknowns are the values of the potential in the airfoil panels, while the unknowns in the finite differences method are the values of the potential in the whole mesh. Thus, the number of unknowns in the latter method is considerably bigger than in the first one, leading to bigger systems of equations that need more time to be solved.

- However, for high final simulation times or small time step sizes, the modified Hariharan-Ping-Scott method is the fastest one. This happens because, despite of having to calculate more unknowns for every instant, it has as advantage that it is not necessary to compute the influence of the whole history before (or the 'recent' one), as in the vortex-lattice method. In other words, the potential at t^n can be calculated just from the potential at t^{n-1} and t^{n-2} and the values of w_p at t^n, whereas in the vortex-lattice method the potential at t^n has to be computed from a lot of instants before, making the latter method to run very slow.

To summarize all the aspects commented above, it can be said that both methods converge equally with Δt, but the modified Hariharan-Ping-Scott runs faster for long simulations because it is not necessary to compute all the history before, compensating the fact of having to calculate more unknowns.

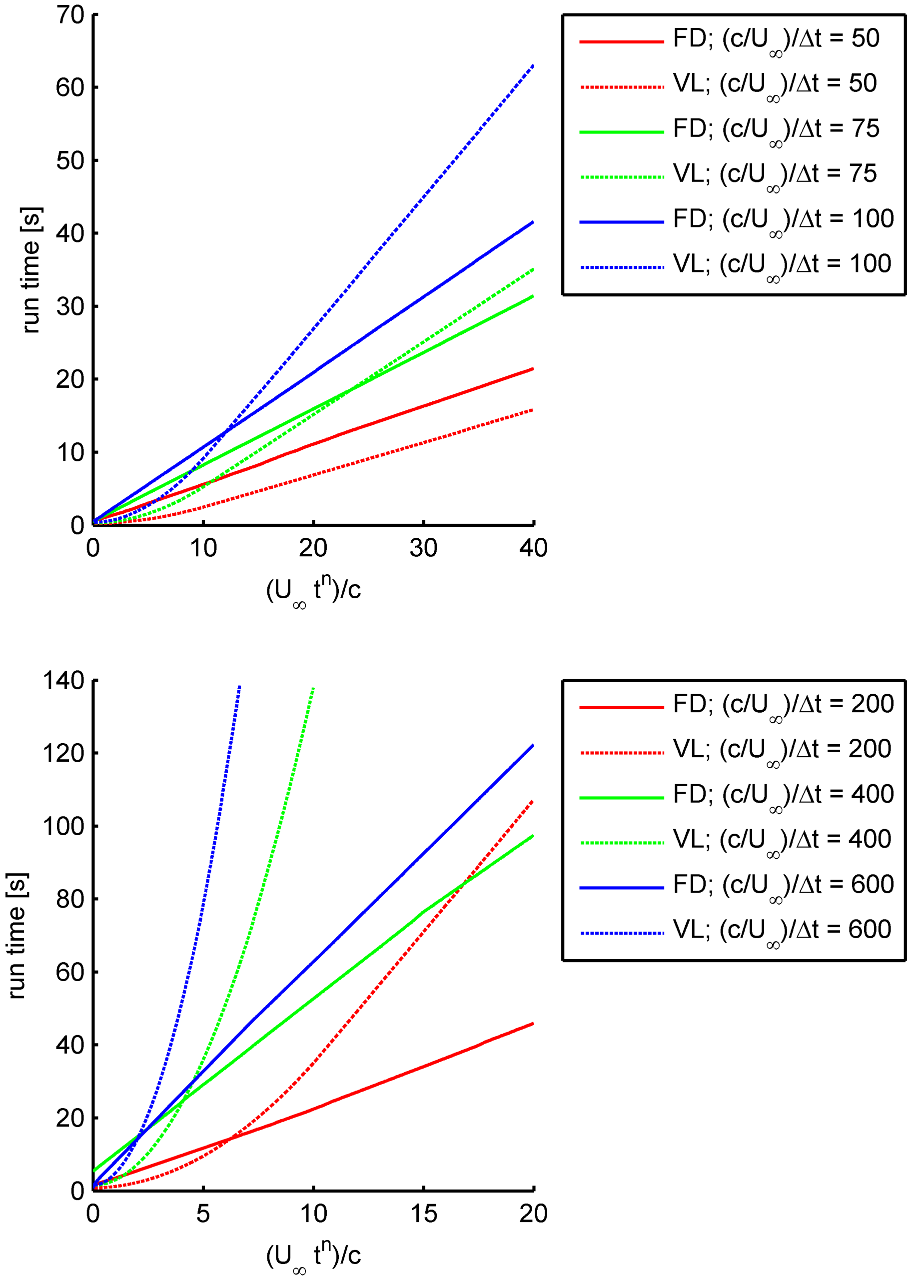

Figure 2.15: Effect of Δt in the total run time.

2.6. Wake patterns calculation

The program described before allows a rough calculation of the wake patterns. Indeed, when the potential ϕ^n_{ij} is computed at every point of the mesh, the horizontal and vertical perturbation velocities u^n_{ij} and v^n_{ij} at every grid point can be obtained by finite differences, taking into account that:

$$u^n_{ij} = \left[\frac{\partial\phi}{\partial x}\right]^{t^n}_{x_i,y_j}, \quad v^n_{ij} = \left[\frac{\partial\phi}{\partial y}\right]^{t^n}_{x_i,y_j}$$

From this and using the antisymmetry of the perturbation velocity field, the values of u and v can be calculated at any point (not necessarily a grid one) by bilinear interpolation of the u^n_{ij} and v^n_{ij} values at the four adjacent nodes.

Now imagine that a drop of ink is injected at the trailing edge at an instant t^n. As the perturbation velocities at that point (say u^n_{te}, v^n_{le}) are known from the potential, the position of that drop of ink at the following instant can be computed from the following explicit formulas:

$$\begin{aligned} x^{n+1}_{ink} &= c + (U_\infty + u^n_{te})\,\Delta t \\ y^{n+1}_{ink} &= v^n_{te}\Delta t \end{aligned}$$

Notice that the upstream velocity is added to the horizontal perturbation velocity to calculate the total horizontal speed at the trailing edge. Knowing the new position of the drop of ink at t^{n+1}, the velocities over that drop can be obtained, as said before, by interpolation of the velocities at the grid points. Thus, the position of the drop at t^{n+2} will be:

$$\begin{aligned} x^{n+2}_{ink} &= x^{n+1}_{ink} + \left(U_\infty + u(t^{n+1}, x^{n+1}_{ink}, y^{n+1}_{ink})\right)\Delta t \\ y^{n+2}_{ink} &= y^{n+1}_{ink} + v(t^{n+1}, x^{n+1}_{ink}, y^{n+1}_{ink})\Delta t \end{aligned}$$

The position at the following instants can be obtained in a similar way. Therefore, the whole wake pattern can be obtained by injecting an imaginary drop of ink at the trailing edge every instant and following the displacements of all the drops.

The obtained results for harmonic motion at three different Mach numbers are shown in figure 2.16, where it can be seen that they are not smooth enough. This is due to the facts that viscosity has not been considered and that the velocity field is calculated assuming always that the wake is placed in the x axis, and not taking into account its real position. Indeed, it is shown in reference [6] that, at least for $M_\infty = 0$, if these two facts are considered, the obtained wake pattern is very smooth and very similar to those obtained experimentally by Bratt [5]. However, it is more convenient to have a formulation based on vorticity (such as the vortex-lattice method), and not in the potential ϕ, to consider these two facts and to get smooth results. Since an equivalence exists between potential and vorticity [6], a method that calculates the latter from ϕ and uses then the vortical-wake formulation is suggested for future developments.

Nevertheless, the results shown in figure 2.16 provide, at least, a qualitative behaviour of the wake. As seen there, the main change in the patterns takes place from $M_\infty = 0.2$ to $M_\infty = 0.4$, i.e., when compressibility starts to be noticed[3]. Below and above that range,

[3] The incompressible approximation is valid when $M^2_\infty \ll 1$.

the patterns look very similar. In general, it can be said that the compressibility makes the patterns decrease their amplitude and become smoother. A better study of the effect of the compressibility and other parameters (such as the oscillation frequency) in that patterns is proposed for future developments.

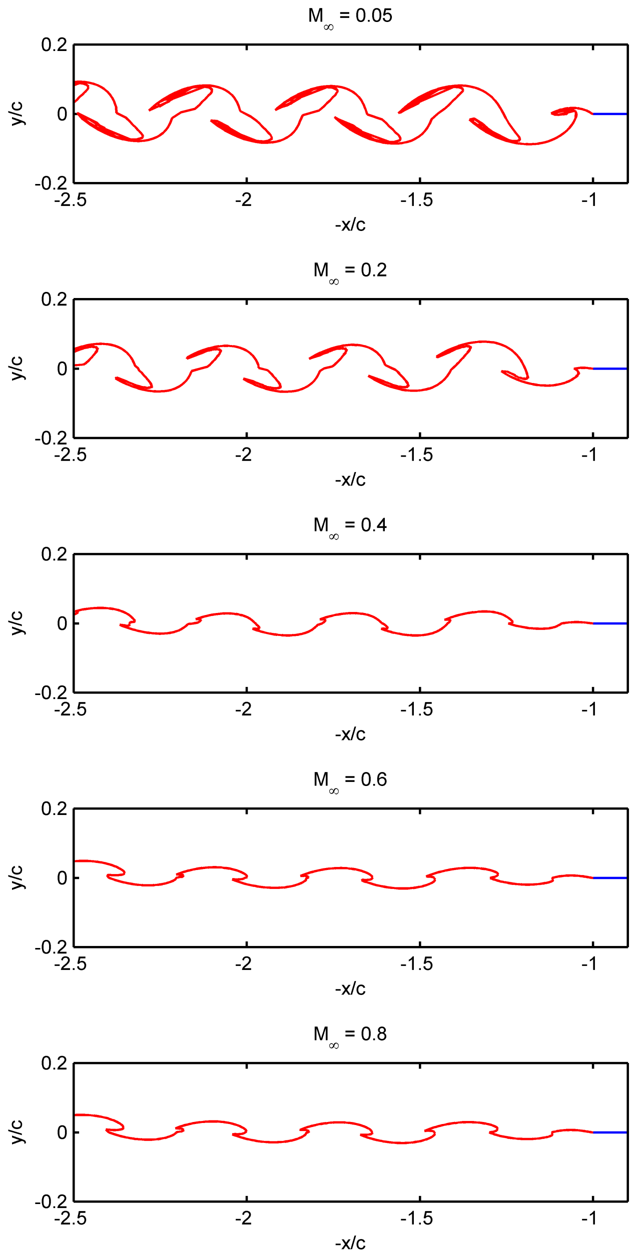

Figure 2.16: Wake patterns for different Mach numbers and a harmonic motion of parameters: $\tilde{h}/c = 0.019, \tilde{\alpha} = 0$ and $\omega c/U_\infty = 17.1578$. The flow goes from right to left.

Chapter 3

Coupling of airfoil dynamics with the modified Hariharan-Ping-Scott method

3.1. Introduction

In the previous chapter, a finite differences method that calculated the forces over an airfoil was described. In order for that method to work, the vertical movement of the airfoil, described by the position of its camber line $z_p = z_p(t, x)$, had to be given as an input. This was useful for solving some problems of interest in unsteady aerodynamics, like the Wagner's, Theodorsen's and Küssner's ones, where the airfoil's motion is known and to calculate the forces over the airfoil is of interest.

However, the vertical movement of the airfoil is just the unknown in some typical problems in aeroelasticity. For example, consider an airfoil like the one shown in figure 3.1, that is submitted to an incident flow U_∞ and is attached to a fixed point through springs and dampers. If the airfoil is in static equilibrium and suffers a small perturbation, it will start oscillating with unknown damping ratio (positive or negative) and frequency. Since that airfoil may represent the typical section of a three-dimensional wing, it is of interest to calculate the airfoil's response given its mechanical properties and the flow conditions in order to prevent phenomenons like flutter or divergence.

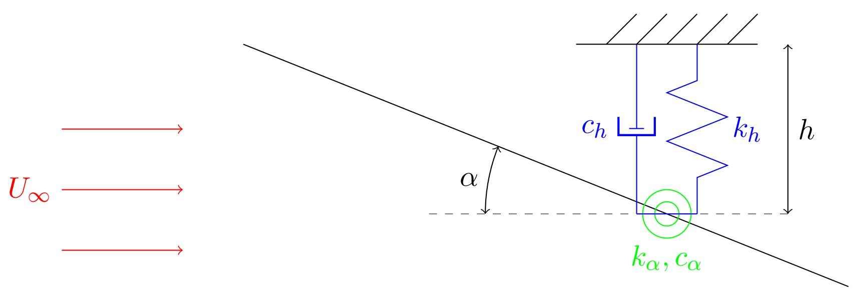

Figure 3.1: Typical section of a wing represented by a rigid airfoil attached to a fixed point by springs and dampers.

In that and many other examples, the airfoil's motion depends on the aerodynamic forces (apart from the inertial, damping, elastic and any other external ones) and vice versa. Thus, in order to compute the response of the airfoil, it is necessary to couple the modified Hariharan-Ping-Scott method, which gives the aerodynamic forces by means of the airfoil's movement, with the airfoil movement's law, which provides an equation for the displacements by means of the actuating forces. This leads to a scheme that will be called *coupled Hariharan-Ping-Scott method*, *coupled HPS method* or *coupled finite differences method* and that is presented first in section 3.2. Later, some simple problems are solved in section 3.3 with that method in order to validate it and to provide some insight of possible applications.

3.2. Description of the coupled Hariharan-Ping-Scott method

3.2.1. Main concepts

In a general case, the chamber line of the airfoil can be described in terms of m known shape functions $\psi_k(x)$ and m generalized coordinates $q_k(t)$ whose evolutions along the time are unknown[1]:

$$z_p(t,x) = \phi_k(x)q_k(t)$$

From the definition of $w_p(t,x)$ (equation (2.6)), it follows that:

$$w_p(t,x) = \psi_k\dot{q}_k + U\frac{\partial\psi_k}{\partial x}q_k - w_g(t,x)$$

In this method, the fluid domain has to be discretized into a grid in the same way that happened with the method described in the previous chapter, and all the vectors $\boldsymbol{\phi}$, $\mathbf{w_p^n}$, etc. keep their meaning. According to this and to the latter equation, the vector that contains the induced velocities over the airfoil can be written as:

$$\mathbf{w_p^n} = \mathbf{W_u}\mathbf{u}^n - \mathbf{w_g^n}$$

where:

$$\begin{aligned}
\mathbf{W_u} &= \left[\begin{array}{ccc|ccc}
U_\infty\dfrac{\partial\psi_1(x_{i_{le}})}{\partial x} & \cdots & U_\infty\dfrac{\partial\psi_m(x_{i_{le}})}{\partial x} & \psi_1(x_{i_{le}}) & \cdots & \psi_m(x_{i_{le}}) \\
\vdots & \ddots & \vdots & \vdots & \ddots & \vdots \\
U_\infty\dfrac{\partial\psi_1(x_{i_{te}})}{\partial x} & \cdots & U_\infty\dfrac{\partial\psi_m(x_{i_{te}})}{\partial x} & \psi_1(x_{i_{te}}) & \cdots & \psi_m(x_{i_{te}})
\end{array}\right] \\
\mathbf{u}^n &= \left[\begin{array}{ccc|ccc} q_1(t^n) & \ldots & q_m(t^n) & \dot{q}_1(t^n) & \ldots & \dot{q}_m(t^n)\end{array}\right]^T \\
\mathbf{w_g^n} &= \left[\begin{array}{ccc} w_g(t^n, x_{i_{le}}) & \ldots & w_g(t^n, x_{i_{te}})\end{array}\right]^T
\end{aligned}$$

If the equation above is substituted into (2.10), it follows that:

$$\mathbf{B_0}\boldsymbol{\phi}^n - \mathbf{B_p}\mathbf{W_u}\mathbf{u}^n = \mathbf{B_1}\boldsymbol{\phi}^{n-1} + \mathbf{B_2}\boldsymbol{\phi}^{n-2} - \mathbf{B_p}\mathbf{w_g^n} \tag{3.1}$$

Notice that, at an instant t^n, the unknowns are $\boldsymbol{\phi}^n$, that contains the values of the potential in the grid points at that instant, and $\mathbf{u}^n$, that contains the current values

[1] Again, repeated index means summation.

of the generalized coordinates and velocities. Since the latter equation was enough for calculating $\boldsymbol{\phi}^n$ when the movement of the airfoil (i.e., $\mathbf{u}^n$) was known, now there are $2m$ more unknowns and therefore $2m$ more equations are needed. Those equations come from the movement's law of the airfoil which, generally, is linear and can be written in the form:

$$m_{ij}\ddot{q}_j(t^n) + c_{ij}\dot{q}_j(t^n) + k_{ij}q_j(t^n) = Q_i^{aero}(t^n) + Q_i^{ext}(t^n)$$

where m_{ij}, c_{ij} and k_{ij} are the components of the constant mass, damping and stiffness matrixes (say $\mathbf{M}, \mathbf{C}, \mathbf{K}$, respectively), whereas Q_i^{aero} and Q_i^{ext} are the components of the aerodynamic and external[2] generalized forces. The latter relation can be transformed into the following system of first-order differential equations:

$$\begin{aligned} \frac{dq_i}{dt} &= \dot{q}_i \\ m_{ij}\frac{d\dot{q}_j}{dt} &= -k_{ij}q_j - c_{ij}\dot{q}_j + Q_i^{aero} + Q_i^{ext} \end{aligned}$$

Using now the definition of $\mathbf{u}^n$, the system above reads as:

$$\mathbf{M}^*\frac{d\mathbf{u}^n}{dt} = \mathbf{K}^*\mathbf{u}^n + \mathbf{I_Q}\left(\mathbf{Q^n_{aero}} + \mathbf{Q^n_{ext}}\right) \tag{3.2}$$

where:

$$\begin{aligned} \mathbf{M}^* &= \begin{bmatrix} \mathbf{I}_{m\times m} & \mathbf{0}_{m\times m} \\ \mathbf{0}_{m\times m} & \mathbf{M} \end{bmatrix} \\ \mathbf{K}^* &= \begin{bmatrix} \mathbf{0}_{m\times m} & \mathbf{I}_{m\times m} \\ -\mathbf{K} & -\mathbf{C} \end{bmatrix} \\ \mathbf{I_Q} &= \begin{bmatrix} \mathbf{0}_{m\times m} \\ \mathbf{I}_{m\times m} \end{bmatrix} \\ \mathbf{Q^n_{aero}} &= [Q_1^{aero}(t^n), \ldots, Q_m^{aero}(t^n)]^T \\ \mathbf{Q^n_{ext}} &= \left[Q_1^{ext}(t^n), \ldots, Q_m^{ext}(t^n)\right]^T \end{aligned}$$

and where $\mathbf{I}_{m\times m}$ and $\mathbf{0}_{m\times m}$ are the identity and the null matrixes of dimensions $m \times m$, respectively.

The vector $\mathbf{Q^n_{aero}}$ that appears in equation (3.2) depends on the unknown $\boldsymbol{\phi}^n$. Indeed, the relation (1.11) can be approximated by:

$$\begin{aligned} Q_i^{aero}(t^n) \simeq\ & \underbrace{2\rho_\infty \int_0^c \frac{\phi(t^n, x, 0^+) - \phi^{up}(t^{n-1}, x, 0^+)}{\Delta t}\psi_i dx}_{=I_1} - \\ & \underbrace{2\rho_\infty U_\infty \int_0^c \phi(t^n, x, 0^+)\frac{d\psi}{dx}dx}_{=I_2} + 2\rho_\infty U_\infty \psi_i(c)\phi^n_{ite} \end{aligned}$$

At the same time, the term I_1 can be approximated by the trapezoidal rule, leading to:

$$I_1 = \rho_\infty \left(\Delta x\right)_I \psi_i(x_I)\frac{\phi_I^n - \phi_I^{n-1}}{\Delta t}$$

[2]External forces encompass any forces that are not inertial, damping, elastic or aerodynamic ones.

where $I = i_{le}, \dots, i_{te}$ and:

$$(\Delta x)_I = \begin{cases} x_{I+1} - x_I; & I = i_{le} \\ x_{I+1} - x_{I-1}; & I = i_{le}+1, \dots, i_{te}-1 \\ x_I - x_{I-1}; & I = i_{te} \end{cases}$$

Similarly, the term I_2 reads as[3]:

$$I_2 = \rho_\infty U_\infty \left(\Delta x\right)_I \psi_i'(x_I)\phi_I^n$$

Taking this into account, the vector $\mathbf{Q^n_{aero}}$ can be written in the following matricial form:

$$\mathbf{Q^n_{aero}} = \mathbf{Q_0^*}\left(\boldsymbol{\phi}^n - \boldsymbol{\phi}^{n-1}\right) - \mathbf{Q_1^*}\boldsymbol{\phi}^n + \mathbf{Q_2^*}\boldsymbol{\phi}^n$$

with:

$$\mathbf{Q_0^*} = \frac{\rho_\infty}{\Delta t} \begin{array}{c} \begin{array}{ccccccc} 1 & \dots & i_{le} & \dots & i_{te} & \dots & N_\phi \end{array} \\ \left[\begin{array}{cc|ccc|cc} 0 & 0 & (\Delta x)_{i_{le}}\,\psi_1(x_{i_{le}}) & \cdots & (\Delta x)_{i_{te}}\,\psi_1(x_{i_{te}}) & 0 & 0 \\ \vdots & \vdots & \vdots & \ddots & \vdots & \vdots & \vdots \\ 0 & 0 & (\Delta x)_{i_{le}}\,\psi_m(x_{i_{le}}) & \cdots & (\Delta x)_{i_{te}}\,\psi_m(x_{i_{te}}) & 0 & 0 \end{array}\right] \end{array}$$

$$\mathbf{Q_1^*} = \rho_\infty U_\infty \begin{array}{c} \begin{array}{ccccccc} 1 & \dots & i_{le} & \dots & i_{te} & \dots & N_\phi \end{array} \\ \left[\begin{array}{cc|ccc|cc} 0 & 0 & (\Delta x)_{i_{le}}\,\psi_1'(x_{i_{le}}) & \cdots & (\Delta x)_{i_{te}}\,\psi_1'(x_{i_{te}}) & 0 & 0 \\ \vdots & \vdots & \vdots & \ddots & \vdots & \vdots & \vdots \\ 0 & 0 & (\Delta x)_{i_{le}}\,\psi_m'(x_{i_{le}}) & \cdots & (\Delta x)_{i_{te}}\,\psi_m'(x_{i_{te}}) & 0 & 0 \end{array}\right] \end{array}$$

$$\mathbf{Q_2^*} = 2\rho_\infty U_\infty \begin{array}{c} \begin{array}{ccccc} 1 & \dots & i_{te} & \dots & N_\phi \end{array} \\ \left[\begin{array}{cc|c|cc} 0 & 0 & \psi_1(c) & 0 & 0 \\ \vdots & \vdots & \vdots & \vdots & \vdots \\ 0 & 0 & \psi_m(c) & 0 & 0 \end{array}\right] \end{array}$$

or, in a more compact way:

$$\mathbf{Q^n_{aero}} = \mathbf{Q_0}\boldsymbol{\phi}^n + \mathbf{Q_1}\boldsymbol{\phi}^{n-1} \tag{3.3}$$

where $\mathbf{Q_0} = \mathbf{Q_0^*} - \mathbf{Q_1^*} + \mathbf{Q_2^*}$ and $\mathbf{Q_1} = -\mathbf{Q_0^*}$. All of these matrixes are sparse.

Finally, consider the following finite difference approximation for the term $d\mathbf{u}^n/dt$ that appears in equation (3.2):

$$\frac{d\mathbf{u}^n}{dt} \simeq \frac{3\mathbf{u}^n - 4\mathbf{u}^{n-1} + \mathbf{u}^{n-2}}{2\Delta t} \tag{3.4}$$

If relations (3.3)-(3.4) are substituted now into (3.2), it follows that:

$$-\mathbf{I_Q}\mathbf{Q_0}\boldsymbol{\phi}^n + \left(\frac{3\mathbf{M}^*}{2\Delta t} - \mathbf{K}^*\right)\mathbf{u}^n = \mathbf{I_Q}\mathbf{Q_1}\boldsymbol{\phi}^{n-1} + \mathbf{M}^*\frac{4\mathbf{u}^{n-1} - \mathbf{u}^{n-2}}{2\Delta t} + \mathbf{I_Q}\mathbf{Q^n_{ext}}$$

The latter matricial equation, altogether with the relation (3.1), provide a system of $N_\phi + 2m$ scalar equations for $N_\phi + 2m$ scalar unknowns, which are the components of $\boldsymbol{\phi}^n$

[3] Consider that $\frac{d\psi_i}{dx} = \psi_i'$.

and $\mathbf{u}^n$. That system can be written in the following form:

$$\begin{bmatrix} \mathbf{B_0} & -\mathbf{B_p W_u} \\ -\mathbf{I_Q Q_0} & \dfrac{3\mathbf{M}^*}{2\Delta t} - \mathbf{K}^* \end{bmatrix} \begin{bmatrix} \boldsymbol{\phi}^n \\ \mathbf{u}^n \end{bmatrix} = \begin{bmatrix} \mathbf{B_1} & \mathbf{0}_{N_\phi \times 2m} \\ \mathbf{I_Q Q_1} & \dfrac{2\mathbf{M}^*}{\Delta t} \end{bmatrix} \begin{bmatrix} \boldsymbol{\phi}^{n-1} \\ \mathbf{u}^{n-1} \end{bmatrix} +$$
$$\begin{bmatrix} \mathbf{B_2} & \mathbf{0}_{N_\phi \times 2m} \\ \mathbf{0}_{2m \times N_\phi} & -\dfrac{\mathbf{M}^*}{2\Delta t} \end{bmatrix} \begin{bmatrix} \boldsymbol{\phi}^{n-2} \\ \mathbf{u}^{n-2} \end{bmatrix} + \begin{bmatrix} -\mathbf{B_p} \\ \mathbf{0}_{2m \times N_p} \end{bmatrix} \mathbf{w_g^n} + \begin{bmatrix} \mathbf{0}_{N_\phi \times m} \\ \mathbf{I_Q} \end{bmatrix} \mathbf{Q_{ext}^n} \quad (3.5)$$

where N_p is the number of grid points located in the airfoil. Also, the system above reads as:

$$\mathbf{C_0} \boldsymbol{\Upsilon}^n = \mathbf{C_1} \boldsymbol{\Upsilon}^{n-1} + \mathbf{C_2} \boldsymbol{\Upsilon}^{n-2} + \mathbf{C_g} \mathbf{w_g^n} + \mathbf{C_Q} \mathbf{Q_{ext}^n} \quad (3.6)$$

where $\boldsymbol{\Upsilon}^n = [\boldsymbol{\phi}^n, \mathbf{u}^n]^T$ is a vector that contains all the unknowns, and where the values of $\mathbf{C_0}$, $\mathbf{C_1}$, $\mathbf{C_2}$, etc. can be easily derived by comparing with equation (3.5).

3.2.2. Computation of the first instants

The formula (3.6) is valid for a general instant t^n, where the values of the solution at the previous instants t^{n-1} and t^{n-2} are known. Thus, the calculation of the solution at the first instants have to be considered apart.

Let the perturbation from the equilibrium position —which is given by the initial conditions $q_k(0)$, $\dot{q_k}(0)$— take place at $t^0 = 0$. For previous instants $t^n < t^0$, $\boldsymbol{\phi}^n$ and $\mathbf{u}^n$ can be assumed to be zero but, when the airfoil moves at $t^n = t^0$, the fluid flow is perturbed and the potential starts to be non-null. Its value at the grid points can be obtained by making $\boldsymbol{\phi}^{n-2} = \boldsymbol{\phi}^{n-1} = \mathbf{0}$ in the expression (3.1):

$$\boldsymbol{\phi}^0 = \mathbf{B_0} \backslash \left[\mathbf{B_p} \left(\mathbf{W_u} \mathbf{u}^0 - \mathbf{w_g^0} \right) \right]$$

Notice that $\mathbf{u}^0$ is not un unknown for this instant, yet is given by the initial conditions:

$$\mathbf{u}^0 = [q_1(0), \ldots, q_m(0), \dot{q_1}(0), \ldots, \dot{q_m}(0)]^T$$

A possible way to proceed now could be to assume $\boldsymbol{\Upsilon}^{-1} = \mathbf{0}$ and $\boldsymbol{\Upsilon}^0 = [\boldsymbol{\phi}^0, \mathbf{u}^0]^T$ and to start integrating from t^1 using expression (3.6). However, the sudden change of the conditions q_k, $\dot{q_k}$ leads to sudden change of the potential $\boldsymbol{\phi}^n$ that, at the same time, leads to high values of the aerodynamic forces at $t = 0$. These high values can provoke another fast changes in the displacements/velocities of the airfoil, in a way that the values of $q_k(t)$, $\dot{q_k}(t)$ are not close to the initial conditions $q_k(0)$, $\dot{q_k}(0)$ when $t \simeq 0$ (see figure 3.2).

Although this procedure may represent correctly the physics of the problem, it has been understood here that $q_k(0)$, $\dot{q_k}(0)$ are the initial conditions for the final movement, not perturbations that lead to second fast changes in $q_k(t)$, $\dot{q_k}(t)$ that, in turn, stay as initial conditions for the final movement.

To make $q_k(0)$, $\dot{q_k}(0)$ be the initial conditions for the final movement, let the airfoil stay in its perturbed state for a lapse of time Δt between $t^{-1} = -\Delta t$ and $t^0 = 0$, instead for a punctual instant t^0. In that case:

$$\begin{aligned}
\boldsymbol{\phi}^{-1} &= \mathbf{B_0} \backslash \left[\mathbf{B_p} \left(\mathbf{W_u} \mathbf{u}^0 - \mathbf{w_g^0} \right) \right] \\
\boldsymbol{\phi}^{0} &= \mathbf{B_0} \backslash \left[\mathbf{B_1} \boldsymbol{\phi}^{-1} + \mathbf{B_p} \left(\mathbf{W_u} \mathbf{u}^0 - \mathbf{w_g^0} \right) \right] \\
\mathbf{u}^{-1} &= \mathbf{u}^0
\end{aligned}$$

With this, $\boldsymbol{\Upsilon}^{-1}$ and $\boldsymbol{\Upsilon}^{0}$ can be computed and the marching-time method governed by (3.6) can be started.

As an example, figure 3.2 shows the vertical displacement h of a rigid airfoil obtained with the two different approaches explained above. The initial conditions were $h(0) = 0.025$ and $\dot{h}(0) = 0$. As can be seen, with the second approach —where the airfoil is forced to stay in its perturbed state for a lapse of time Δt before $t = 0$—, the initial evolution of $h(t)$ is smoother, tends to $h(0)$ when $t \to 0$ and its slope $\dot{h}(t)$ is also zero at $t = 0$. Also, the results converge with those obtained with the coupled Hernandes-Soviero method described in [6]. However, with the first approach —where the airfoil is in its perturbed state just for a punctual instant—, the results are not that accurate, $h(t)$ presents a quasi-step change for h in the initial instants (so it does not tend to the initial condition when $t \to 0$) and its slope is not zero at $t = 0$.

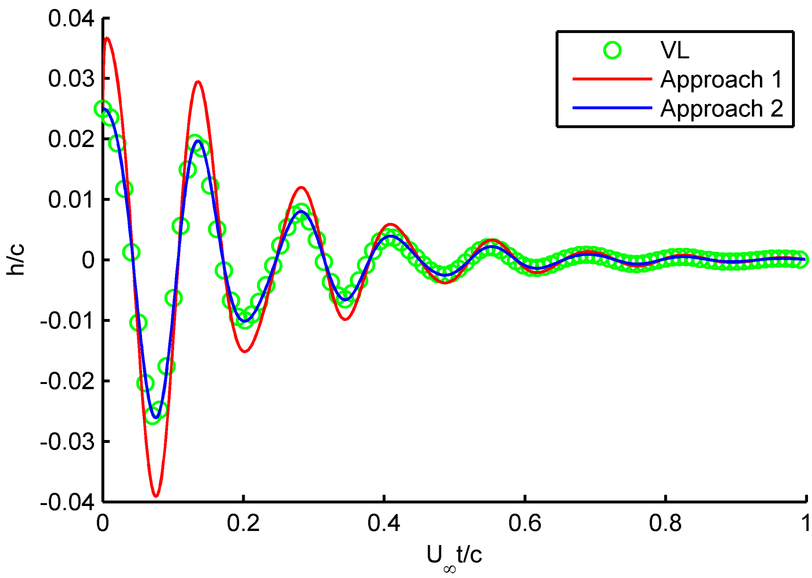

Figure 3.2: Illustration of the effect of the two different approaches.

3.2.3. Efficient scheme implementation. Summary of all the steps

As it happened with the finite difference method of the previous chapter, a system of equations has to be solved for every simulated instant t^n and the matrix of that system ($\mathbf{C_0}$) is constant, very big and sparse. Thus, a LU factorization with rows and columns permutations can be used again to accelerate the scheme. In this case:

$$\mathbf{P}'\mathbf{C_0}\mathbf{Q}' = \mathbf{L}'\mathbf{U}' \tag{3.7}$$

Here, the prime symbol is used to avoid confusions with the matrixes that took part in the LU decomposition used in the previous chapter for the modified HPS method. Following the same reasoning as the one presented in section 2.2.3, it is possible to define the permuted vector of unknowns $\hat{\boldsymbol{\Upsilon}}^n$ as $\boldsymbol{\Upsilon}^n = \mathbf{Q}'\hat{\boldsymbol{\Upsilon}}^n$ and to compute it by solving the two triangular systems that appear in the following equation:

$$\hat{\boldsymbol{\Upsilon}}^n = \mathbf{U}' \backslash \left(\mathbf{L}' \backslash \left(\hat{\mathbf{C_1}} \hat{\boldsymbol{\Upsilon}}^{n-1} + \hat{\mathbf{C_2}} \hat{\boldsymbol{\Upsilon}}^{n-2} + \hat{\mathbf{C_g}} \mathbf{w_g^n} + \hat{\mathbf{C_Q}} \mathbf{Q_{ext}^n} \right) \right) \tag{3.8}$$

where $\hat{\mathbf{C_1}} = \mathbf{P}'\mathbf{C_1}\mathbf{Q}'$, $\hat{\mathbf{C_2}} = \mathbf{P}'\mathbf{C_2}\mathbf{Q}'$, $\hat{\mathbf{C_g}} = \mathbf{P}'\mathbf{C_g}$ and $\hat{\mathbf{C_Q}} = \mathbf{P}'\mathbf{C_Q}$.

Once $\hat{\boldsymbol{\Upsilon}}^n$ is calculated, the values of $\mathbf{u}^n$ can be extracted from it. Indeed, since $\mathbf{u}^n$ corresponds to the last $2m$ rows of $\boldsymbol{\Upsilon}^n$ and $\boldsymbol{\Upsilon}^n = \mathbf{Q}'\hat{\boldsymbol{\Upsilon}}^n$, $\mathbf{u}^n$ can be obtained by multiplying the submatrix formed by the last $2m$ rows of $\mathbf{Q}'$ (say $\mathbf{U}_{\hat{\Upsilon}}$) by $\hat{\boldsymbol{\Upsilon}}^n$, i.e.:

$$\mathbf{u}^n = \mathbf{U}_{\hat{\boldsymbol{\Upsilon}}} \hat{\boldsymbol{\Upsilon}}^n \tag{3.9}$$

where:

$$\left(\mathbf{U}_{\hat{\boldsymbol{\Upsilon}}}\right)_{ij} = \left(\mathbf{Q}'\right)_{N_\phi+i,j}, \quad i = 1, \ldots, 2m, \quad j = 1, \ldots, N_\phi + 2m$$

In order to clarify all the ideas before, the method has been summarized in the following steps:

- Input data:
  - Flow conditions: ρ_∞, U_∞, a_∞ and $w_g(t, x)$.
  - Mesh and time simulation data: x_i, y_j, c, Δt and t_f.
  - Mass, damping and stiffness matrixes ($\mathbf{M}$, $\mathbf{C}$, $\mathbf{K}$), initial conditions ($q_k(t = 0)$, $\dot{q}_k(t = 0)$) and external generalized forces ($Q_k^{ext}(t)$).
  - Shape functions $\psi_k(x)$ and their derivatives $\psi_k'(x)$.
- First, compute matrixes $\mathbf{A_0}$ and $\mathbf{A_1}$ as pointed in section 2.2.2; then, calculate $\mathbf{B_0}$, $\mathbf{B_1}$, $\mathbf{B_2}$ and $\mathbf{B_p}$ as shown in section 2.2.1; and finally, construct matrixes $\mathbf{C_0}$, $\mathbf{C_1}$, $\mathbf{C_2}$, $\mathbf{C_g}$ and $\mathbf{C_Q}$ as explained in section 3.2.1.
- Perform the LU factorization of $\mathbf{C_0}$ with rows and columns permutations (equation (3.7)).
- Permute $\mathbf{C_0}$, $\mathbf{C_1}$, $\mathbf{C_2}$, $\mathbf{C_g}$ and $\mathbf{C_Q}$ to obtain $\hat{\mathbf{C_0}}$, $\hat{\mathbf{C_1}}$, $\hat{\mathbf{C_2}}$, $\hat{\mathbf{C_g}}$ and $\hat{\mathbf{C_Q}}$ as indicated just after equation (3.8). Obtain $\mathbf{U}_{\hat{\boldsymbol{\Upsilon}}}$ as well.
- Assume $t^n = \Delta t$, calculate $\boldsymbol{\Upsilon}^{-1}$, $\boldsymbol{\Upsilon}^0$ as pointed in section 3.2.2 and obtain $\hat{\boldsymbol{\Upsilon}}^{-1} = \mathbf{Q}' \backslash \boldsymbol{\Upsilon}^{-1}$, $\hat{\boldsymbol{\Upsilon}}^0 = \mathbf{Q}' \backslash \boldsymbol{\Upsilon}^0$.
  - Evaluate $\hat{\boldsymbol{\Upsilon}}^n$ using equation (3.8).
  - Extract the generalized coordinates and velocities from $\hat{\boldsymbol{\Upsilon}}^n$ through relation (3.9).
  - Actualize variables:

$$\hat{\boldsymbol{\Upsilon}}^{n-2} \leftarrow \hat{\boldsymbol{\Upsilon}}^{n-1}, \quad \hat{\boldsymbol{\Upsilon}}^{n-1} \leftarrow \hat{\boldsymbol{\Upsilon}}^n, \quad t^n \leftarrow t^n + \Delta t$$

3.3. Results

In order to validate the method described before and to provide simple examples of possible applications, it has been tested with three problems: (i) the flutter point calculation of a rigid flat airfoil with two degrees of freedom, (ii) the flutter point calculation of a flexible cantilevered panel and (iii) the response to a sharp-edge gust of a rigid airfoil with free vertical displacement.

In the first two cases, the flutter Mach number M_f has been calculated as a function of the upstream sound speed a_∞ and the results have been compared with other ones provided by the coupled Hernandes-Soviero method described in reference [6], getting excellent agreement. No other references to compare with have been found in the available literature, hence, the results presented here are original or not well-known.

For the third problem, some results have been found in the literature (in reference [20], for example). However, they are not useful for this work because they offer a very extensive study of the influence of many parameters, and the aim of this section is just to show simple examples that could provide some insight into possible applications of the coupled HPS method. Thus, the few simple results obtained here will be only validated with the coupled vortex-lattice method.

3.3.1. Flutter of a rigid airfoil

Consider a rigid airfoil attached to a fixed point with springs and dampers like the one shown in figure 3.1. The mechanical properties of the system are given by the airfoil's mass m_a, the x-coordinate of its gravity centre x_g, the x-coordinate of the elastic axis x_e, the inertia I_e about that axis, the stiffness constants k_h, k_α of the linear and torsional springs (respectively) and the damping constants c_h, c_α of the linear and torsional dampers (respectively as well).

If the same degrees of freedom used for the Theodorsen's problem (as shown in figures 2.5 and 3.1) are employed now, the airfoil's equations of motion read as [9]:

$$\begin{bmatrix} m_a & m_a(x_g - x_e) \\ m_a(x_g - x_e) & I_e \end{bmatrix} \begin{bmatrix} \ddot{h} \\ \ddot{\alpha} \end{bmatrix} + \begin{bmatrix} c_h & 0 \\ 0 & c_\alpha \end{bmatrix} \begin{bmatrix} \dot{h} \\ \dot{\alpha} \end{bmatrix} + \begin{bmatrix} k_h & 0 \\ 0 & k_\alpha \end{bmatrix} \begin{bmatrix} h \\ \alpha \end{bmatrix} = \begin{bmatrix} Q_h^{aero} \\ Q_\alpha^{aero} \end{bmatrix}$$

It has to be reminded that h and α are measured respect from the equilibrium position. The latter equation provides the mass, damping and stiffness matrixes. On the other hand, the shape functions associated with the degrees of freedom are:

$$\begin{aligned} \psi_h(x) &= -1 \\ \psi_\alpha(x) &= x_e - x \end{aligned}$$

Typically, the parameters of the airfoil are described in terms of the following non-dimensional variables:

$$\mu = \frac{m_a}{\rho_\infty \pi b^2}, \quad x_\alpha = \frac{x_g - x_e}{b}, \quad a = \frac{x_e - b}{b}, \quad r_\alpha^2 = \frac{I_e}{m_a b^2}$$

where $b = c/2$ is the semi-chord of the airfoil. Also, the natural frequencies that the airfoil would have if it could only experiment vertical or rotational motion are used:

$$\omega_h = \sqrt{\frac{k_h}{m_a}}, \quad \omega_\alpha = \sqrt{\frac{k_\alpha}{I_e}}$$

Once the parameters of the airfoil are fixed, the flutter speed can be obtained just by a trial and error procedure. First, a flow speed U_∞ is assumed and the airfoil's motion is computed. If the oscillations' amplitude decreases (increases), the airfoil's motion is calculated again for a higher (lower) flow speed. This is done until a flow speed that makes the amplitude keep constant (i.e., the flutter speed) is found.

The results obtained for an airfoil of parameters $\mu = 2$, $x_\alpha = 0.4$, $a = -0.4$, $r_\alpha^2 = 0.25$, $\omega_h/\omega_\alpha = 0.6$ and no damping are presented in figure 3.3. As can be seen there, the flutter Mach number increases when the upstream sound speed decreases, until the latter reaches a minimum value. From that point, M_f and a_∞ both increase. Also, it can be observed that the results provided by this coupled finite differences method show excellent agreement with the ones provided by the coupled vortex-lattice method described in [6]. In addition, the solution obtained by neglecting compressibility effects [6] —which is given by the equation $M_f a_f = U_f^{inc} = const.$, where U_f^{inc} is the flutter speed in incompressible regime— has been also represented to check that the solution obtained by the coupled HPS method tends asymptotically to it when $M_\infty \to 0$.

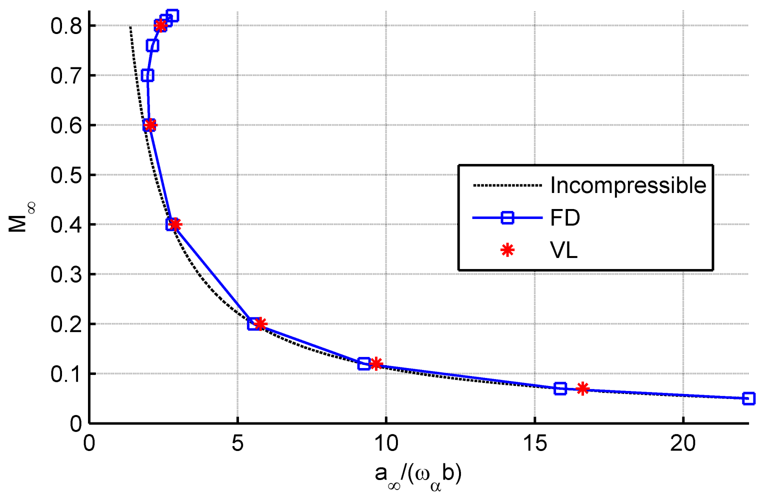

Figure 3.3: Flutter Mach number M_f as a function of the upstream sound speed a_∞ for a rigid airfoil.

At the same time, the response of the airfoil at $M_\infty = 0.6$ and different upstream velocities is shown in figure 3.4. In the case where U_∞ is equal to the flutter speed U_f, it can be seen how the oscillations keep their amplitude constant after an initial perturbation takes the airfoil away from its equilibrium position ($h = 0$, $\alpha = 0$). In the cases where U_∞ is greater or lower than the flutter speed, the amplitude of the oscillations decrease or increase, respectively.

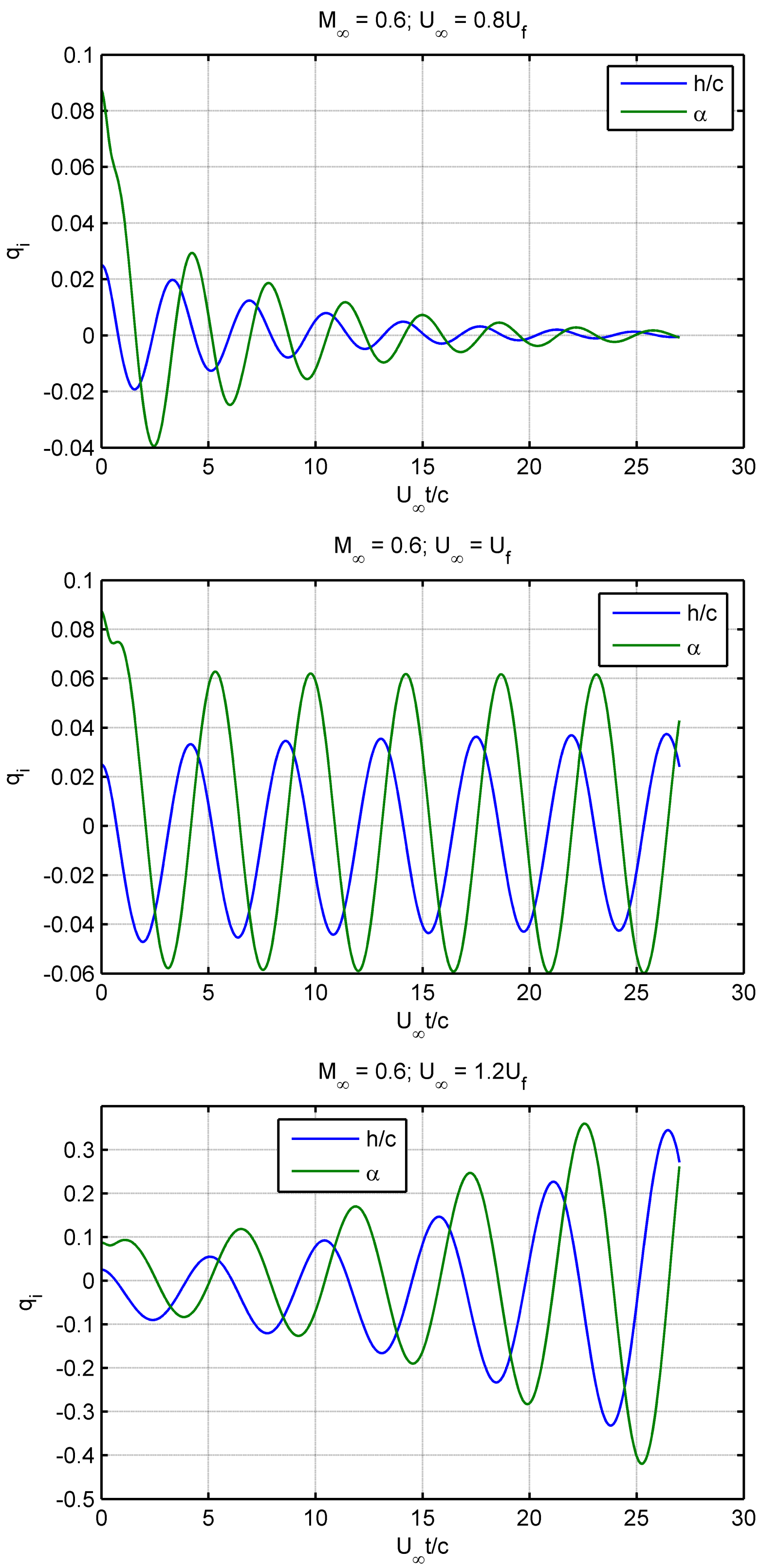

Figure 3.4: Evolution of the degrees of freedom along the time for U_∞ values that are lower, equal and greater than the flutter speed U_f.

3.3.2. Flutter of a cantilevered flexible plate

Now consider a cantilevered flexible flat plate, like the one shown in figure 3.5, whose dimensions are $L \times H$. Let the incident flow come in the direction given by L and $H \to \infty$ in order to simulate a two-dimensional problem.

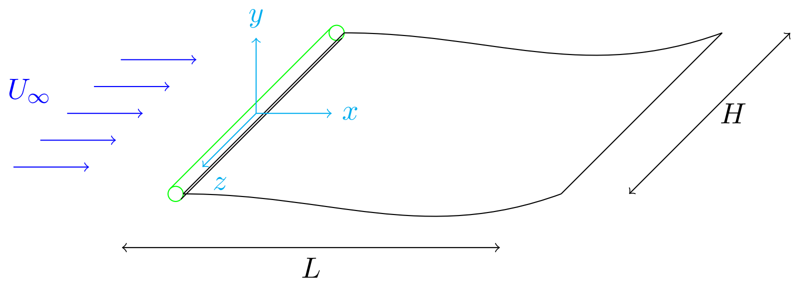

Figure 3.5: Scheme of a cantilevered flexible plate submitted to an incident flow.

The equation that governs the displacements of the mean line $z_p(t,x)$ of the plate is [8]:

$$\sigma \frac{\partial^2 z_p}{\partial t^2} + D \frac{\partial^4 z_p}{\partial x^4} = \Delta p \tag{3.10}$$

where σ is the superficial mass density, D is the flexural rigidity and Δp is the pressure difference between the lower and the upper parts of the plate. At the same time, D is given by:

$$D = \frac{E h_p^3}{12(1-\nu^2)}$$

where E is the Young's modulus, h_p the plate thickness and ν the Poisson's coefficient.

At the same time, the displacements of the mean line can be described by a Galerkin decomposition:

$$z_p(t,x) = \sum_{i=1}^{m} \hat{q}_i(t)\hat{\psi}_i(x)$$

where $\hat{\psi_1}(x), \ldots, \hat{\psi_m}(x)$ are the first m *in vacuo* vibration modes, and $\hat{q_1}(t), \ldots, \hat{q_m}(t)$ are the corresponding generalized coordinates. These modes are obtained in reference [2] and read as:

$$\begin{aligned} \hat{\psi}_i(x) = {} & [\sin(\beta_i L) - \sinh(\beta_i L)]\,[\sin(\beta_i x) - \sinh(\beta_i x)] + \ldots \\ & [\cos(\beta_i L) + \cosh(\beta_i L)]\,[\cos(\beta_i x) - \cosh(\beta_i x)] \end{aligned} \tag{3.11}$$

where $\beta_1 < \beta_2 < \ldots$ are the different solutions of:

$$\cos(\beta_i L)\cosh(\beta_i L) + 1 = 0$$

The modes described by (3.11) have as drawback that involve calculations of hyperbolic sines and cosines. Thus, when a few modes are employed and the different values of β_i start increasing, those hyperbolic sines and cosines become very high and introduce numerical errors. In order to avoid them, these modes can be divided by $e^{2\beta_i L}$, limiting then their maximum value. For that purpose, define first the following functions:

$$\begin{aligned}
\mathcal{S}(x) &= \frac{\sin x}{e^x} \\
\mathcal{C}(x) &= \frac{\cos x}{e^x} \\
\mathcal{S}_h(x) &= \frac{\sinh x}{e^x} = \frac{1-e^{-2x}}{2} \\
\mathcal{C}_h(x) &= \frac{\cosh x}{e^x} = \frac{1+e^{-2x}}{2}
\end{aligned}$$

It is very important to define $\mathcal{S}_h(x)$ as $(1-e^{-2x})/2$ and not as $\sinh x/e^x$, so the computer never calculates the term $\sinh x$, which is the one that introduces the numerical errors. The same can be said for $\mathcal{C}_h(x)$. Using this functions, some proportional modes $\psi_i^*(x)$ can be defined as:

$$\psi_i^*(x) = \frac{\hat{\psi}_i(x)}{e^{2\beta_i L}} = e^{-\beta_i(L-x)} \left[\left[\mathcal{S}(\beta_i L) - \mathcal{S}_h(\beta_i L) \right] \left[\mathcal{S}(\beta_i x) - \mathcal{S}_h(\beta_i x) \right] + \dots \right.$$
$$\left. \left[\mathcal{C}(\beta_i L) + \mathcal{C}_h(\beta_i L) \right] \left[\mathcal{C}(\beta_i x) - \mathcal{C}_h(\beta_i x) \right] \right]$$

Again, the latter modes present a problem, which is that some of them have bigger values than others, so they have more weight in the simulations and lead newly to numerical errors. To solve this inconvenient, the following integral can be performed symbolically:

$$I_i^* = \frac{1}{L} \int_0^L (\psi_i^*)^2 dx$$

which allows to define new proportional modes:

$$\psi_i(x) = \frac{\psi_i^*(x)}{\sqrt{I_i^*}}$$

These modes verify that the integrals of their square powers are all the same:

$$\int_0^L \psi_i^2 dx = \frac{1}{I_i^*} \int_0^L (\psi_i^*)^2 dx = L$$

Thus, they can be expected to have similar values and similar weight in the simulation.

Now, let z_p be described in terms of the latter modes and their corresponding generalized coordinates q_i:

$$z_p(t,x) = \sum_{i=1}^{m} \psi_i(x) q_i(t) \tag{3.12}$$

It can be shown that those modes verify:

$$\frac{d^4\psi_i}{dx^4} = \beta_i^4 \psi_i \tag{3.13}$$

$$\int_0^L \psi_i \psi_j dx = 0 \qquad (i \neq j) \tag{3.14}$$

Using expressions (3.12)-(3.14), equation (3.10) provides the following matricial relation:

$$\begin{bmatrix} \sigma L & & \\ & \ddots & \\ & & \sigma L \end{bmatrix} \begin{bmatrix} \ddot{q}_1 \\ \vdots \\ \ddot{q}_m \end{bmatrix} + \begin{bmatrix} D\beta_1^4 L & & \\ & \ddots & \\ & & D\beta_m^4 L \end{bmatrix} \begin{bmatrix} q_1 \\ \vdots \\ q_m \end{bmatrix} = \begin{bmatrix} Q_1^{aero} \\ \vdots \\ Q_m^{aero} \end{bmatrix}$$

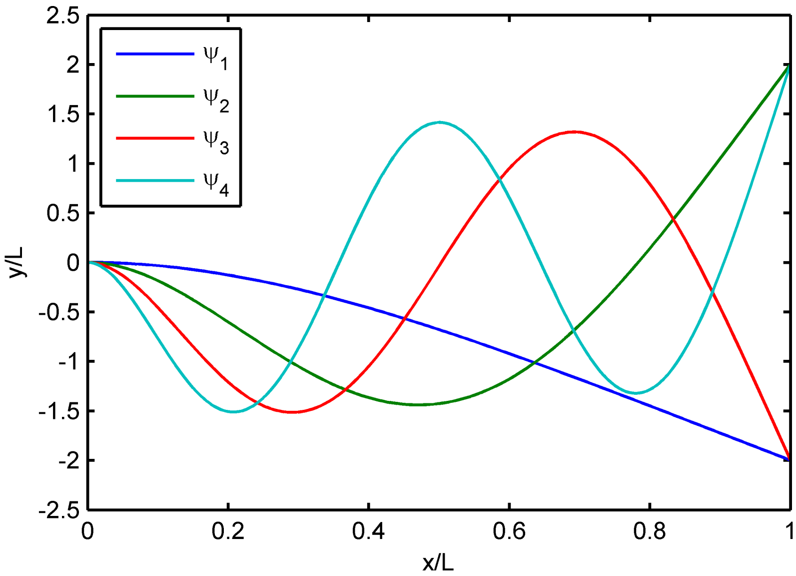

Figure 3.6: In vacuo vibration mode used for the Galerkin decomposition.

which, at the same time, gives the expressions of the mass and stiffness matrixes.

In order to reduce the number of parameters, the following dimensionless variables will be introduced:

$$M^* = \frac{\rho_\infty L}{\sigma}, \quad U^* = \sqrt{\frac{\sigma}{D}} L U_\infty, \quad a^* = \sqrt{\frac{\sigma}{D}} L a_\infty$$

The results obtained for a plate with $M^* = 0.6$ are plotted in figure 3.7. It can be seen that the flutter Mach number depends on the upstream sound speed a_∞ in a similar way than in the case of a rigid airfoil (figure 3.3): the slope of the curve $M_f - a_\infty$ is almost vertical for low values of a_∞ and it starts decreasing later for bigger values of a_∞. In that figure, the solution obtained by neglecting compressibility effects [6] —which is again given by the equation $M_f a_\infty = U_f^{inc} = const$— is also represented. As expected, the curve $M_\infty - a_\infty$ obtained with the coupled HPS method tends asymptotically to the above mentioned curve corresponding to incompressible flow when $M_\infty \to 0$.

On the other hand, figure 3.8 shows the evolution of the generalized coordinates along the time when the plate flutters at $M_f = 0.4$. Again, it can be seen that the oscillations keep their amplitude constant, as expected.

In addition, the evolution of the flutter mode with the Mach number is plotted in figure 3.9. It can be observed that, for low Mach numbers, the flutter modes present a neck at $x/L \simeq 0.7$ that is a consequence of the combination of the first two *in vacuo* modes (see figure 3.6). For higher Mach numbers, that neck disappears and the flutter mode looks more similar to the first *in vacuo* mode than to a combination of the first two modes.

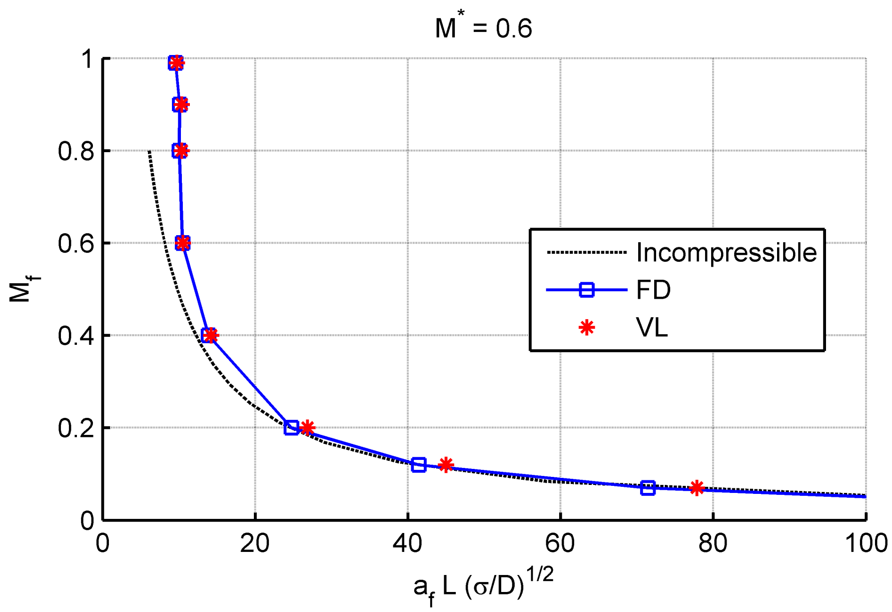

Figure 3.7: Dependency of the flutter Mach number M_f with the upstream sound speed a_∞ for a flexible plate.

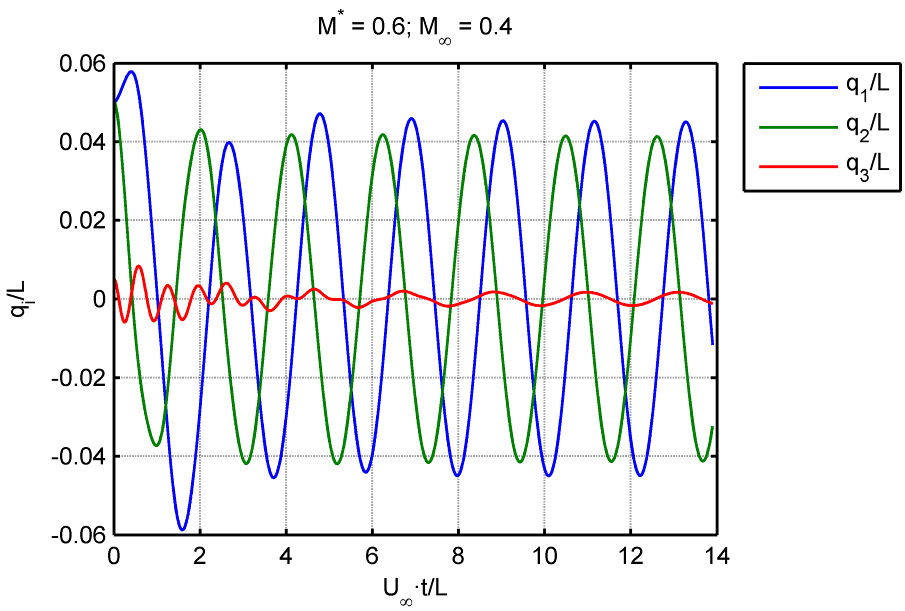

Figure 3.8: Evolution of the generalized coordinates along the time when the flexible airfoil flutters.

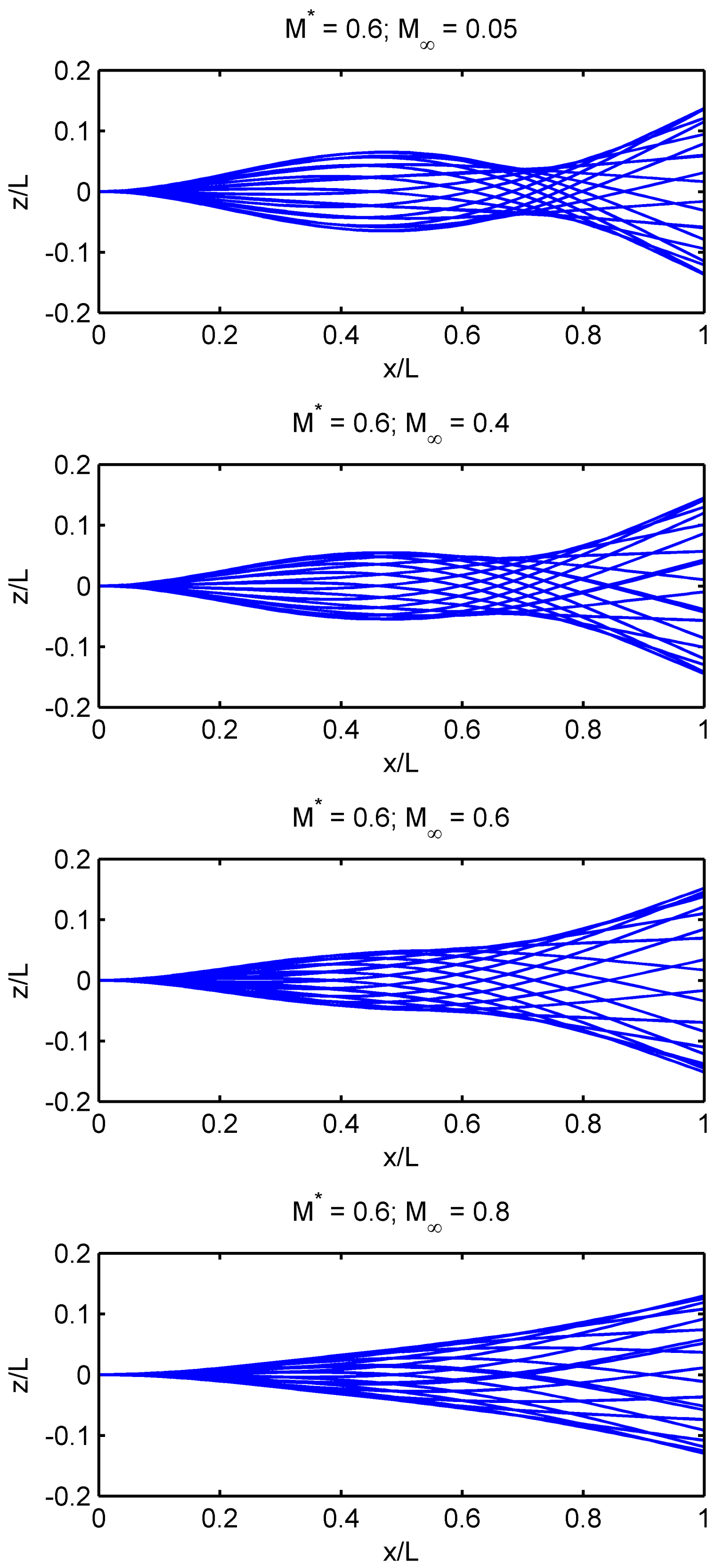

Figure 3.9: Flutter mode for different Mach numbers and $M^* = 0.6$.

Finally, as a way to check the quality of the results, the flutter mode obtained numerically for $M^* = 0.74$ and incompressible regime is compared in figure 3.10 with the one obtained experimentally by Eloy and others [8]. As can be seen, both modes look very similar, only being a slight discrepancy in the size of the neck. This happens due to two facts: first, the plate used in the experiment is not two-dimensional and, second, the displacements are not really small, so non-linear effects should be taken into account to get more accuracy. Indeed, a good proof of the non-linearity is that the plate does not always have its trailing edge at $x = L$ when it flutters, as supposed in the numerical method, because its length has to be approximately constant. Anyway, the results show that the coupled HPS method seems to be accurate and reliable.

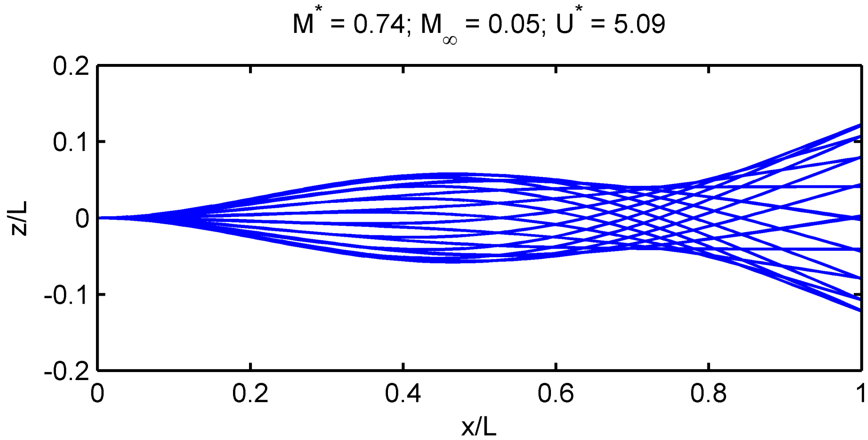

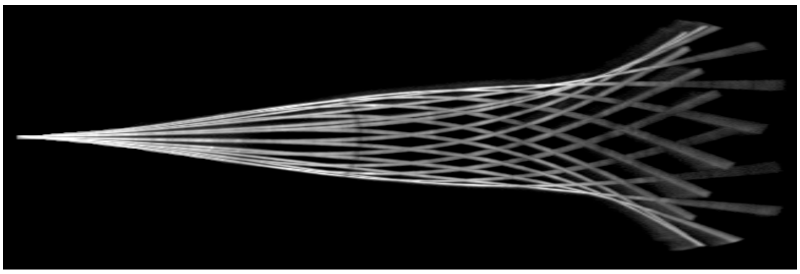

Figure 3.10: Comparison of the flutter mode obtained experimentally (below) and with the coupled HPS method (above) for incompressible flow.

3.3.3. Response to a vertical sharp-edge gust

Let an airfoil that is flying at constant horizontal speed U_∞ enter in a vertical sharp-edge gust of intensity $w_0 = U_\infty$, as shown in figure 3.11. As a consequence of the gust, the airfoil will experiment extra lift (see Küssner's problem, section 2.3.3) and will start moving up. The horizontal speed is assumed to keep being U_∞. If rotation and deformation of the airfoil are neglected for simplicity reasons, the movement will be described by the equation:

$$m_a \ddot{\eta} = Q_\eta^{aero}$$

where m_a and η are the mass and the vertical displacement of the airfoil, respectively. The shape function associated with η is:

$$\psi_\eta(x) = 1$$

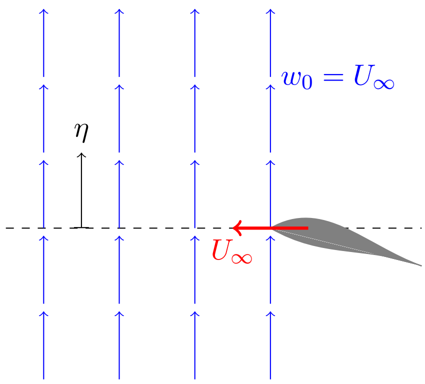

Figure 3.11: Airfoil entering in a vertical sharp-edge gust of speed $w_0 = U_\infty$.

Figure 3.12 shows the airfoil vertical velocity as a function of the elapsed time. Again, the results show good agreement between the coupled finite differences and the coupled vortex-lattice methods. For all Mach numbers, the vertical speed increases at the beginning due to the extra lift caused by the gust. As that vertical speed becomes bigger, the total induced speed over the airfoil decreases, as well as the effective angle of attack (see figure 3.13), causing the total lift over the airfoil to diminish. After some time, the vertical speed is exactly the same as the gust speed, so there are not any induced velocities over the airfoil, there is not any lift as well and therefore the airfoil stays with that speed. That is why $\dot{\eta}/U_\infty \to 1$ in all the curves.

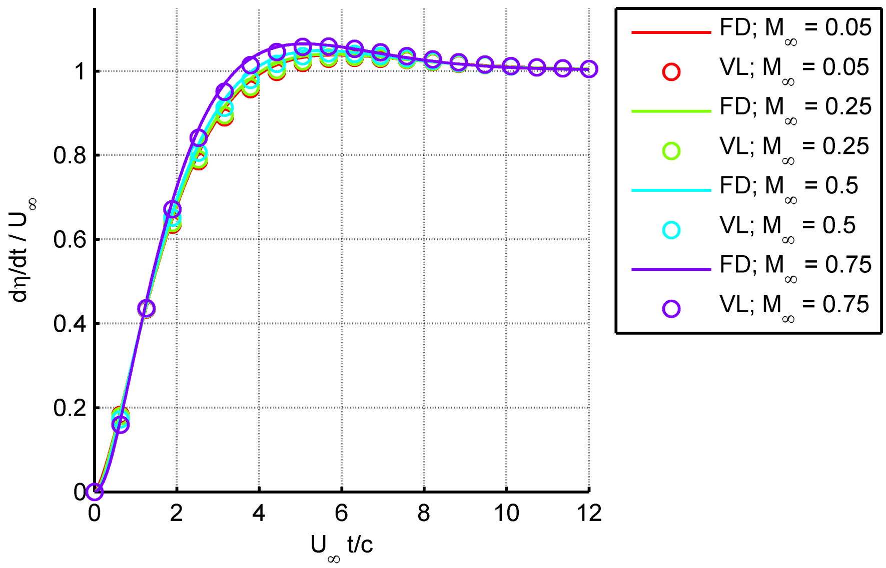

Figure 3.12: Vertical speed of the airfoil $\dot{\eta}$ as a function of the elapsed time.

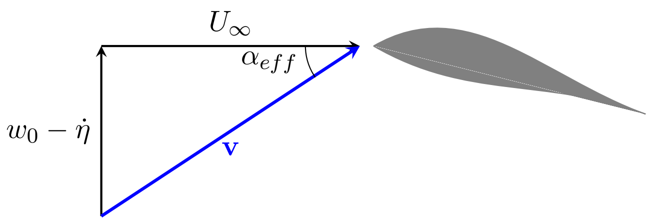

Figure 3.13: Scheme that illustrates the total incident flow velocity (blue) over the airfoil, and the effective angle of attack α_{eff}. The horizontal component is U_∞, whereas the vertical one is the difference between the gust speed w_0 and the airfoil's vertical velocity $\dot{\eta}$. Hence, when the latter is equal to the first, the effective angle of attack is null and the lift tends to zero as time increases.

Conclusions and future developments

In this work, two improvements have been proposed to the Hariharan-Ping-Scott method [11] —a finite differences marching-time scheme that calculates the two-dimensional unsteady linearized potential flow past an airfoil. The first consists in employing a non-uniform mesh to focus more points near the airfoil, which is the origin of the convected waves, clearly accelerating the convergence of the solution. The second relies on using a BDF implicit time integration scheme, making the algorithm much more stable and allowing to take bigger time step sizes.

The scheme modified with those improvements, which has been renamed as *modified Hariharan-Ping-Scott method*, is only valid for problems where the airfoil motion is known. Thus, to make it useful for solving aeroelasticity problems where the airfoil motion is just the unknown, such as flutter, it has been coupled with the airfoil dynamics in a way that is valid for any airfoil (flexible or rigid, cantilevered or hinged, etc.) that presents a linear equation of motion. This coupling has proved to be accurate and has also provided results that have not been found in the available literature, such as the flutter of a flexible cantilevered panel.

Also, the efficiency of the modified Hariharan-Ping-Scott method and the modified Hernandes-Soviero method's —a vortex-lattice scheme presented by Hernandes and Soviero [12][13] modified with a truncation algorithm proposed by Colera and Pérez-Saborid [6]— have been compared. For short simulations, the modified Hernandes-Soviero method has proved to be the fastest one because the number of unknowns (the potential at the airfoil points) is lower. However, for long simulations, the modified Hariharan-Ping-Scott method is the fastest one because, despite of the bigger number of unknowns (the potential at the whole mesh, not only in the airfoil points), it does not have to calculate the influence of great part of the history before, as it happens in the Hernandes-Soviero method.

The latter conclusion can be extended out of the unsteady aerodynamics field to say that, in general, finite differences methods can be faster than boundary element methods when solving the two-dimensional wave equation in the time domain[4]. Indeed, since two-dimensional waves have a dissipative nature, a wave that is generated at any point will always affect to all the space inside its wavefront. Thus, for solving any 2D wave equation in the time domain with a boundary element method —such as the vortex-lattice— it is necessary to store the whole evolution of the variables at the boundaries —or part of it if

[4]Of course, boundary elements methods may present other advantages respect finite differences methods, but they are not going to be analysed here.

a truncation method is used— and to calculate its influence at every instant, leading to memory and slowness problems. However, as commented before, finite differences methods do not need to store all or great part of the history before and therefore they do not present those problems. In return, a bigger number of unknowns has to be handled, but this can be done in an efficient way by using adequate sparse matrixes.

Both the modified Hariharan-Ping-Scott method and the coupled one with the airfoil dynamics (renamed as *coupled Hariharan-Ping-Scott method*) have proved to give accurate results in an efficient way. Also, they are useful for any general linear problem, unlike other methods that are only valid for specific cases like harmonic motion or rigid profile. Thus, they can be an excellent tool for preliminary designs, where the CFD conventional programs are too expensive for the required accuracy.

In addition, both methods are very intuitive because they rely on the physics beyond the fundamental equations of the linearized unsteady potential flow theory and do not leave the time domain, unlike the classical approach for the theory, which uses many tedious mathematical developments in the frequency domain. Also, they can be implemented with programs like Matlab, which is accessible to students, has a simple syntax that is easy to understand and also permits an efficient program run. Hence, they can be used as a teaching application.

Some future developments are proposed to improve the commented methods:

- The use of higher-order formulas to approximate both the spatial and the time derivatives. This would provide more accuracy, but it must be done with care because it could also bring stability problems.
- To use an adaptive time step size instead of a fixed one.
- To extend the method for supersonic regime.
- To extend the methods for a three-dimensional domain. However, it has to be remarked that a boundary element method (vortex-lattice, doublet-lattice or any other) could be more efficient for that case because the number of unknowns would be much lower and, as well, it would not be necessary to compute all the history before since three-dimensional waves are non-dispersive (see figure 3.14).

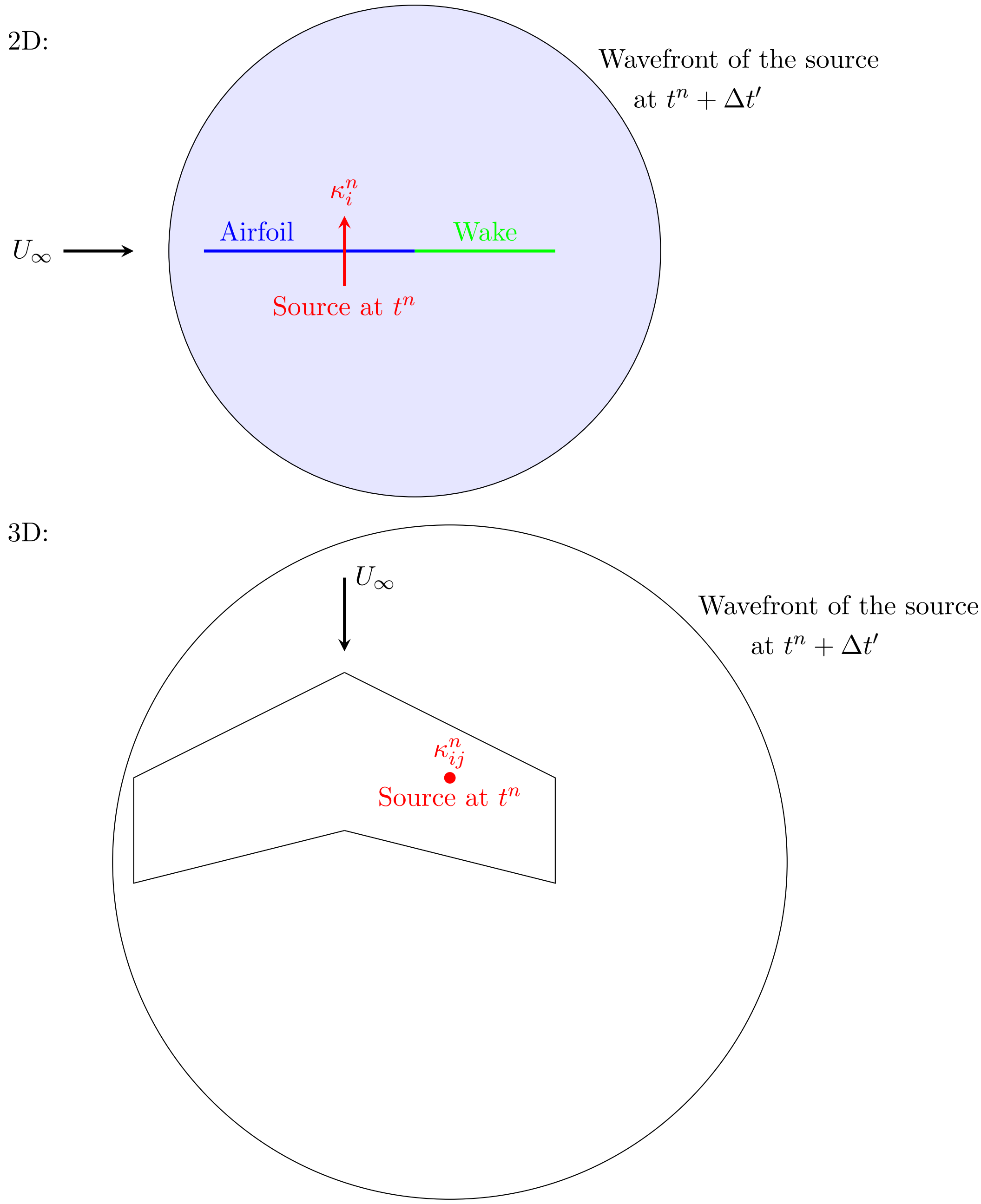

Figure 3.14: Difference between the two-dimensional and three-dimensional cases in doublet-lattice and vortex-lattice methods. When the flow is two-dimensional, any source, doublet, vortex or fundamental solution κ_i^n born at t^n affects to the points at and inside its wavefront. Thus, it is necessary to store its value during all the simulation and to compute its influence at every simulated instant. However, when the flow is three-dimensional, any fundamental solution κ_{ij}^n born at t^n affects only to points situated just at its wavefront. Thus, when the latter goes out of the wing after a time $\Delta t'$, κ_{ij}^n can be erased and its influence does not have to be calculated any more.

Bibliography

[1] E. Alberdi, J.J. Anza: *BDF-α: A Multistep Method with Numerical Damping Control.* Universal Journal of Computational Mathematics 1(3): 96-108, 2013.

[2] S.S. Arora: *Study of Vibration Characteristics of Cantilever Beams of Different Materials.* Thapar University, Patiala, 2012.

[3] R.L. Bisplinghoff, H. Ashley, R.L. Halfman: *Aeroelasticity.* Dover, 1996.

[4] A. Blázquez, M. Pérez-Saborid: Clases de Aeroelasticidad, E.T.S.I. Sevilla, curso 2012-2013.

[5] J.B. Bratt: *Flow Patterns in the Wake of an Oscillating Aerofoil.* Aeronautical Research Council Reports and Memoranda, 2011-2012.

[6] M. Colera, M. Pérez-Saborid: *Cálculo numérico del flujo potencial no estacionario sobre perfiles en los regímenes subsónico y supersónico.* E.T.S.I. Sevilla, 2015.

[7] D. Eberly: *Derivative Approximation by Finite Diferences.* Geometric Tools, LLC, 2015.

[8] C. Eloy, R. Lagrange, C. Souillez, L. Schouvellier: *Aeroelastic instability of cantilevered flexible plates in uniform flow.* Journal of Fluid Mechanichs, Vol 611, pags 97.106, 2006.

[9] Y.C. Fung: *An Introduction to the Theory of Aeroelasticity.* Dover, 2008.

[10] Ü. Gülcat: *Fundamentals of Modern Unsteady Aerodynamics.* Springer, 2010.

[11] S.I: Hariharan, Y. Ping, J.R. Scott: *Time Domain Numerical Calculations of Unsteady Vortical Flows about a Flat Plate Airfoil.* Journal of Computational Physics 101, 419-430, 1992.

[12] F. Hernandes, P.A.O. Soviero: *Unsteady Aerodynamic Coefficients Obtained by a Compressible Vortex-Lattice Method.* Journal of Aircraft, Vol 46, No 4, 2009.

[13] F. Hernandes, P.A.O. Soviero: *A Numerical Model for Thin Airfoils in Unsteady Compressible Arbitrary Motion.* J. of the Braz. Soc. of Mech., Sci. & Eng., 2007.

[14] A. Kayran: *Küssner's Function in the Sharp-Edged Gust Problem - A Correction.* Journal of Aircraft, Vol 43, No 5, 2006.

[15] J. Katz, A. Plotkin: *Low-Speed Aerodynamics.* Cambridge University Press, 2001.

[16] D. Mateescu: *Theoretical solutions for unsteady compressible subsonic flows past oscillating rigid and flexible airfoils*. Mathematics in Engineering, Sciencie and Aerospace, Vol 2 No 1, 2011.

[17] MatLab LU documentation. MathWorks, 2016.

[18] W.J. McGroskey, J. Aircraft, 22(3), 236 (1985).

[19] I.F. Miranda, P.A.O. Soviero: *Inditial Response of Thin Wings in a Compressible Subsonic Flow*. 18th International Congress of Mechanical Engineering, November 6-11, 2005.

[20] M.J. Patil, D.J. Taylor: *Gust Response of Highly Flexible Aircraft*. American Institute of Aeronautics and Astronautics.

[21] T. Theodorsen: *General Theory of Aerodynamic Instability and the Mechanism of Flutter*. NACA Tech. Rep. 496, 1935.